COMPARISON OF EXPERIMENTAL AND THEORETICAL FORCES ON A MODEL DREDGE CUTTERHEAD

A Thesis

by

RUSTY LEE PERMENTER

Submitted to the Office of Graduate Studies of
Texas A&M University
in partial fulfillment of the requirements for the degree of

MASTER OF SCIENCE

December 2010

Major Subject: Ocean Engineering

Comparison of Experimental and Theoretical Forces on a Model Dredge Cutterhead

COMPARISON OF EXPERIMENTAL AND THEORETICAL FORCES ON A MODEL DREDGE CUTTERHEAD

A Thesis

by

RUSTY LEE PERMENTER

Submitted to the Office of Graduate Studies of
Texas A&M University
in partial fulfillment of the requirements for the degree of

MASTER OF SCIENCE

Approved by:

Chair of Committee,	Robert Randall
Committee Members,	Jeffrey Falzarano
	Steven DiMarco
Head of Department,	John Niedzwecki

December 2010

Major Subject: Ocean Engineering

ABSTRACT

Comparison of Experimental and Theoretical Forces on a Model Dredge Cutterhead.

December 2010

Rusty Lee Permenter, B.S., Stephen F. Austin State University

Chair of Advisory Committee: Dr. Robert Randall

Dredging is a critical part of maintaining the nation's ports and harbors that play a major role in international trade. The design of dredge equipment requires knowledge of the forces expected on an average dredge. For a cutter suction dredge one of the largest forces is applied on the cutter head. To determine the design criteria for a given cutter suction dredge the forces on the cutter head must be known.

Forces on a 33 cm (13 inch) model cutter head have been measured using a model cutter suction dredge 10.2 cm ((4 inch)) suction and 3 inch (7.6 cm) discharge) in the Haynes Coastal Engineering Laboratory. The experimental results are compared to the results of a previously developed theory for estimating cutterhead forces. A MATLAB program is written and used to solve the theoretical equations. The sediment used in the study had a d_{50} of 0.27 mm and an angle of internal friction of 21.6°. The sediment is contained in the deep sediment pit 7.6 m (25 ft long), 3.7 m wide(12 ft) and 1.5 m deep(5 ft) in the dredge/tow tank that is 45.7 m long(150 ft), 3.7 m wide(12 ft), and 3.0 m deep(10 ft). The objectives of the study are to calculate the forces using existing theory and MATLAB program and compare the theoretical results to those

measured in the laboratory. The effects of the depth of cut, direction of swing, and cutter rpm on the forces acting on the cutter head are evaluated. The forces on the cutterhead are determined through the use of a set of six load cells rated at 13.3 kN (3000 lb). The load cell measurements allow direct calculation of the forces on the cutter head through the use of static equilibrium equations with the assumption of a constant swing speed. Once the forces are determined the results can be scaled to fit an actual dredge and then be applied in the determination of dredge design characteristics.

The study shows the ability of the theory to determine the forces within an order or magnitude. The theoretical forces allow design of a cutter using a factor of safety. The variability of the forces in the laboratory study shows the assumption that the cutting forces are generally steady is not always valid.

ACKNOWLEDGEMENTS

I would like to thank my committee chair, Dr. Randall, and my committee members, Dr. Falzarano and Dr. DiMarco, for their guidance and support throughout the course of this research. I would also like to thank my fiancé for her support throughout this process. I would also like to thank Po Hung-Yeh, John Reed, and Aaron Drake for their assistance throughout the study.

NOMENCLATURE

α	Blade cutting angle
β	Cut angle
δ	Soil/steel angle of friction
ϕ	Angle of internal friction
b	Width of blade
p_{1m},p_{2m} ,p_{3m}	Pore pressure
g	Gravitational constant
γ	Specific weight of water
H	Cutting depth
D	Depth of cutter
b	Width of blade
n_{cr}^{w}	Critical porosity water
n_1	Initial porosity
κ	Profile angle
h	Height of cut
m	Ratio swing speed over cutter speed
D_c	Layer thickness
r	Distance tooth point to center line of the cutter head
v_s	Swing speed
ω	Cutter angular velocity

F_h	Force in the horizontal
h_i	Thickness of the cut
E	Specific energy required for a cut
Ω_1	Angle covered when cavitation occurs
Ω_0	Total angle covered
Ω	Angle covered by blade
ξ	Top angle of the cutterhead
ι	Angle of blade with axis of cutterhead
v_c	Swing velocity
v_{cir}	Circumferential velocity
e	Volume strain
k_m	Average permeability
c_1,c_2	Non-cavitating cutting coefficient
d_1,d_2	Cavitating cutting coefficient
h_b	Height of blade

TABLE OF CONTENTS

CHAPTER Page

LIST OF FIGURES

FIGURE Page

LIST OF TABLES

CHAPTER I

INTRODUCTION

Dredging

Dredging is a multibillion-dollar industry that spans the globe. International trade spurs most of the industry's business since keeping shipping lanes and ports at authorized depth funds many dredging projects. An additional aspect of the dredging industry is beach nourishment and land reclamation, which uses dredged material to serve as beach fill. In some cases, dredged materials have been used in order to create new islands. Contaminated sediments also require specialized dredging and capping in some cases. The massive amounts of money that these projects cost generate a need for quality research geared toward the optimization of dredging equipment, and standard practices for evaluating dredge performance need to be used. A large number of dredging projects within the United State employ cutter suction dredges. The driving design considerations on a cutter suction dredge are the pump size, the cutter head design, and the winch power. In the past, cutter suction dredges have been constructed based on rule of thumb and previous experience, but as the cost of dredging continues to increase the value of good design theory increases accordingly. Turner (1996)

The main components of a cutter suction dredge are the ladder, cutter, main pump, hull winches, and spuds as shown in Figure 1. The ladder is an articulating arm that holds a cutter head and a suction pipe that allows the sediment being excavated by the

---

This thesis follows the style and format of the *Journal of Dredging Engineering.*

cutterhead to be entrained into the slurry pump system. The slurry is pumped through a pipeline into some type of disposal facility. The spuds of a cutter suction dredge are two pilings that can be raised and lowered to hold the dredge in position. Using the spuds as a pivot point the winches swing the dredge back and forth across the cut. The dredge is advanced by swinging to one side, alternating spuds, swinging back to the other side, and then changing back to the original spud. Some dredges use a spud carriage, which is when a spud is mounted on a mobile track that can be used to advance the dredge without the spuds being changed. This greatly enhances the productivity of a cutter suction dredge. In Figure 2, the position of the spuds and the ladder are shown.

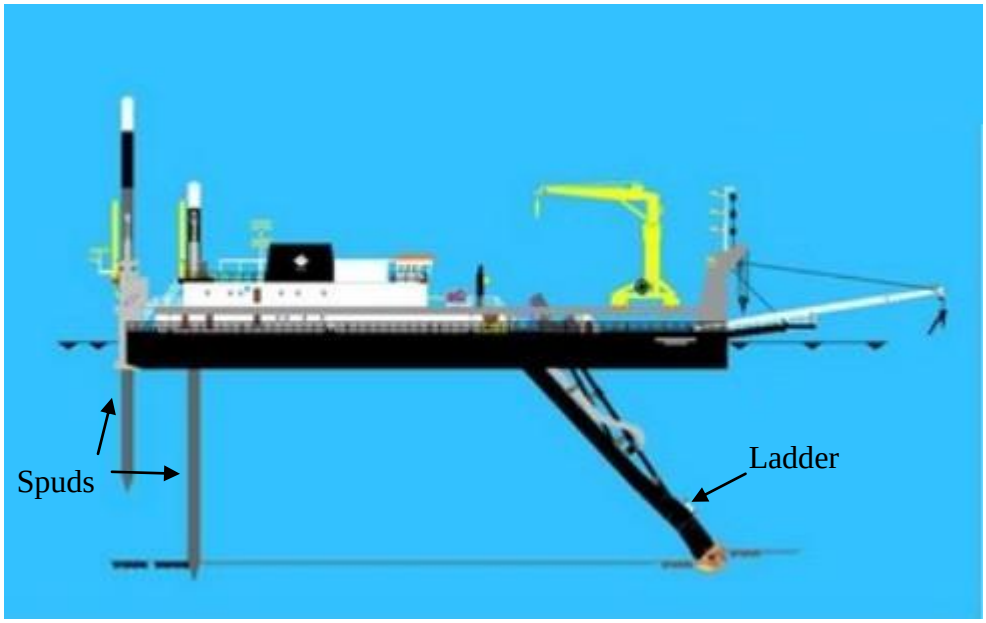

Figure 1. Plans of a Cutter Suction Dredge(Dredging Today)

Properly designing a dredge requires an understanding of the forces being experience by the cutter head. Previous studies have researched the forces on cutter

heads, but the facilities necessary to test the theory are few. This study compares of forces estimated by the theory of Miedema (1987) to experimental results from laboratory testing at the Haynes Coastal Laboratory. The laboratory tests uses varying dredge parameters and the force equations developed by Young (2009) to determine the forces on the cutter for each scenario.

Purpose of Study

The purpose of this research was to compare the measured forces on a model cutter suction dredge using the cutting theory of Miedema (1987). The study will measure the forces on the cutterhead using the force transducers installed on the dredge ladder. The effects of the RPM and cut depth are quantified by varying the two parameters. The forces can then be applied to the design of any cutterhead. The forces on a cutter head depend on many factors acting simultaneously including cutter rpm, depth of cut, angle of cut, swing speed, advancement of the cutter, and the geometry of the cutter head. The study allows for the determination of the influence of the flowrate and SG on the tip of the cutterhead during advancement. A nuclear density meter and a magnetic flowmeter are used to measure slurry density and flowrate. The forces calculated using the theory are compared with the experimental forces on the cutter head using the load cells on the dredge carriage. The variables involved in the theoretical calculations are varied in the laboratory tests to determine the corresponding measured force on the cutterhead for each scenario. These measurements were made in the spring of 2010 during the excavation of the dredge basin. These results are used to verify the cutting theory and further verify the load cell calculations. The results also allow for an

improvement of current cutter theory so that increasingly accurate predictions of the forces on a cutter head can be constructed. As a byproduct of predicting the forces on the cutter head, the location of cavitation on the cutter head blades is calculated since this calculation makes a great difference in the forces experienced by the cutter head and the efficiency of the pump.

A major factor in the forcing on the cutterhead is whether the cutter is overcutting or undercutting. Overcutting occurs when each cutter blade initially penetrates the sediment at the top of the cut. Undercutting occurs when the blade enters the sediment at a horizontal at the bottom of the cut. Overcutting tends to be the most efficient of the two methods. The differences between overcutting and undercutting are demonstrated in the Figure 2. The cutterhead shown rotates counterclockwise so that overcutting occurs from right to left and undercutting occurs during left to right motion.

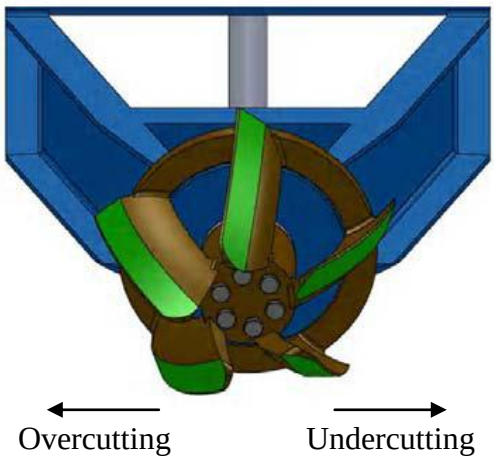

Figure 2. Diagram of Cutterhead at Haynes Laboratory(Young 2009)

The interaction between the sand and the cutter head determines most of the force on the cutter hand and the type of sand is a major cause for differing forces. The various parameters involved with the study of sand require the use of geotechnical studies including the sieve test, direct shear test, and the porosity test. The density of the sand was determined since density can be used to determine any inertial forcing experienced by the cutter blade.

The result of this study is the ability to better model cutter heads using computer tools and also the additional knowledge as to how the dredge carriage works. Additionally, this thesis demonstrates the usefulness of the six load cell configuration in determining the forces applied to the cutterhead which will allow for future studies of scaled cutterheads in the Haynes Coastal Engineering Laboratory.

CHAPTER II

PREVIOUS FORCE STUDIES

A clearer understanding of the factors of the forces on the cutter must be obtained design an effective cutter head. Several studies have attempted to determine the forces on a blade driven through saturated sand through theoretical calculations and used these calculations attempted to calculate the forces on a cutter head. These studies must be investigated to determine what can be built upon or modified to fit this research. Additional studies calculated the forces on a cutter suction head using a dredge carriage equipped with load cells to measure the force on the cutter head. These studies have shown good results and have resulted in a methodology for studying cutter heads that will prove useful in future design projects.

Turner (1996) uses several methods to determine cutting force that can be applied in the field. The line pull can be used to obtain the force on the cutter in calm water due to the fact that the line pull must exceed whatever force the cutter is experiencing. The line pull is generally 1.5 to 1.6 times greater than the cutting force to account for all the forces exerted upon the dredge. The determination of the cutting force can be achieved by observing the point at which the dredge is not accelerating since the force of the winch and the forces at the cutter are equal at this point. The cutter horsepower can also be applied to determine the amount of power needed for certain cutting conditions. Turner (1996) uses the cutter drive horsepower and the RPM to determine the torque required to cut through certain sediment. The following equations are used to calculate the horsepower and torque, respectively:

$$HP = Cutting\,Force * 2\pi\, Cutter\,Radius * \frac{RPM}{550\frac{ft * lbs}{s} * 60\frac{s}{\min}} \tag{2.1a}$$

$$HP = \frac{Torque * RPM}{5250} \tag{2.1b}$$

$$Cutting\ \ Force = \frac{Torque}{Cutter\ \ Radius} \tag{2.2}$$

The great thing about the simple equations is the wealth of data available through such methods. Dredges keep logs dedicated to maximizing production, and this method provides a quick way to determine cutter forces and adjust dredging accordingly. On the other end of the spectrum, several researchers have tried to model the interaction between the sand and the cutter head during dredging operations.

Os. and van Leussen (1987) tackled the issue first with a study on the cutting forces in saturated sand. They applied basic cutting theory to a blade hydraulically pushed through soil at speeds ranging from 0.01 to 5.0 m/s. They concentrated mainly on the forces caused by volumetric strain and pore-water pressure, which means that most of the forces are due to dilatancy. Dilatancy is the decrease in pore pressure due to changing pore volume. This change in pressure results in a change in forcing on the blades. The theory was tested by using a full-scale test and high-speed photography to determine the location of any cavitation. To cover a broad scope of dredging equipment various types of sand and numerous blade angles were used during testing. The blade width throughout the testing was 0.35m. Many of the geotechnical properties of the soil were calculated to determine the forces on the cutting surface. The major components of their theory are the angles alpha (blade angle with the horizontal), beta (average angle of

shear zone with the horizontal), delta (angle of friction between sand and metal surfaces), and phi(the angle of internal friction. By using these coefficients, the following force equations were solved in the horizontal and the vertical directions for a two-dimensional model. The equations are in terms of the specific weight γ, the blade cutting angle α, the shear angle β, the soil/steel angle of friction δ, the angle of internal friction ϕ, depth in meters D, height of cut h, and pore pressures p_1 and p_2.

$$F_h = \gamma bhH[p_1 f_1(\alpha,\beta,\delta,\phi) + p_2 f_2(\alpha,\beta,\delta,\phi) \tag{2.3}$$

$$F_v = \gamma bhH[p_1 f_1(\alpha,\beta,\delta,\phi)\cot g(\alpha+\delta) - p_2 f_2(\alpha,\beta,\delta,\phi)\cot g(\beta+\phi) \tag{2.4}$$

$$H = D + 10(with\,cavitation) \tag{2.5}$$

$$f_1(\alpha,\beta,\delta,\phi) = \frac{\sin(\alpha+\delta)*\sin(\phi)}{\sin(\alpha+\beta+\delta+\phi)} \tag{2.6}$$

$$f_2(\alpha,\beta,\delta,\phi) = \frac{\sin(\beta+\phi)*\sin(\delta)}{\sin(\alpha+\beta+\delta+\phi)} \tag{2.7}$$

$$H = h*\frac{v}{k'}*\frac{n_{cr}^{w} - n_1}{1-n_{cr}^{w}}\ (without\ cavitation) \tag{2.8}$$

Vlasblom (1998) examines the topic of what forces need to be considered during the design of a cutterhead. The results are reached using the assumption of linear theory with respect to the ratios between the cutting depth and the force on the cutter. These ratios allow for a kind of non-dimensionalization of the force equations. The forces are initially determined for a single blade and then transferred to the full cutter head. The tangential force T and radial force R are calculated as follows:

$$T = C\sin(\theta - \varphi) - N\cos\kappa\cos(\theta - \varphi)$$
$$R = C\cos(\theta - \phi) + N\cos\kappa\cos(\theta - \varphi) \quad (2.9)$$

In equation 2.9 C is the cutting force, N is the normal force, theta (θ) represents the angle between the cutting force and the x-axis, kappa (κ) is the angle formed by the perpendicular formed by the surface of revolution, and phi (ϕ) is an angle dependent on tooth position. These values can easily be converted into a horizontal and vertical force. The axial force is defined by the following equation:

$$A = N\sin\kappa \quad (2.10)$$

To determine the force N and C a linear proportionality between the depth of cut and both forces is applied giving the assumed form of the equations:

$$C = a_c + b_c d$$
$$N = a_n + b_n d \quad (2.11)$$

In the previous equations b_c and b_n are the forces per unit depth and the a_c and a_n are the coefficient of the cutting forces. The normal force is related to the cutting force using the following relation:

$$C = a_c - \frac{b_c}{b_n}a_n + \frac{b_c}{b_n}N \quad (2.12)$$

Substituting the equation 2.12 into the previous equations for the tangential and radial forces to get a relationship with respect to C_0, N, θ, φ, and κ. To determine the relationship between θ and φ the relationship between the swing speed m and position must be determined.

$$x_c = r*(m\varphi + \cos\varphi)$$
$$y_c = r*(1+\sin\varphi) \tag{2.13}$$

$$m = \frac{v_s}{\omega r}$$
$$\varphi = \omega t \tag{2.14}$$

Taking the derivative of y_c results in the following formula which is later used in determining the average force on the cutter:

$$\varphi = \theta - \arccos(m\sin\theta) \tag{2.15}$$

For design purposes the mean forces were then calculated by integrating the force over the angle of the cut with respect to various angles Φ_0, Φ_{in}, θ_0, and θ_{in}.

$$\varphi_0 = \arcsin(\frac{D_c}{r} - 1) \tag{2.16}$$

$$\theta_0 = \arctan(\frac{\cos\varphi_0}{m - \sin\varphi_0}) \tag{2.17}$$

$$\theta_{in} = \frac{a_n \frac{\theta_0^2}{2} - b_n \frac{v_s \cos\kappa}{\omega * p}[\theta_0 * \cos\theta_0 - \sin\theta_0]}{a_n - b_n \frac{v_s \cos\kappa}{\omega * p}[\cos\theta_0 - 1]} \tag{2.18}$$

$$\varphi_{in} = \theta_{in} - \arccos(m*\sin(\theta_{in})) \tag{2.19}$$

Equations 2.16-19 are used to determine the mean forces on the cutterhead.

$$\overline{N}_{total} = \frac{p}{2\pi}\{a_n - \frac{b_c}{b_n}\frac{v_s \cos\kappa}{\omega * p}[\cos\theta - 1]\} \tag{2.20}$$

$$\overline{T} = C_0 \sin(\theta_{in} - \varphi_{in}) + \overline{N}_{total}[\frac{b_c}{b_n}\sin(\theta_{in} - \varphi_{in}) - \cos\kappa\cos(\theta_{in} - \varphi_{in})] \tag{2.21}$$

$$\overline{R} = C_0 \cos(\theta_{in} - \varphi_{in}) + \overline{N}_{total}[\frac{b_c}{b_n}\cos(\theta_{in} - \varphi_{in}) - \cos\kappa \sin(\theta_{in} - \varphi_{in})] \quad (2.22)$$

Once again, these forces are converted to an axial coordinate system.

Miedema (1987), whose doctoral dissertation focuses on the subject, has performed the majority of work in the field of cutting theory. The theory focuses on the movement of a solitary blade through sand. The forces on the cutting blade were calculated using the assumption that the majority of the force on the blade is due to dilatancy, which allows other effects due to gravity, cohesive, adhesive and inertial forces to be ignored. This assumption only applies at speeds from 0.5 to 5 m/s due to previous research. For these speeds the horizontal (F_c) and vertical (F_h) forces affecting each blade (in two dimensions) were calculated during both cavitation and non-cavitation based on the cutting force coefficients c_1, c_2, d_1, and d_2, the thickness of the cut h_I, the volume strain e, and the average permeability k_m:

$$F_{vnc} = c_2 * \rho_w * g * v_c * h_i^2 * b * e / k_m \quad (2.23)$$

$$F_{hnc} = c_1 * \rho_w * g * v_c * h_i^2 * b * e / k_m \quad (2.24)$$

$$F_{hca} = d_1 * \rho_w * g * (z + 10) * h_i * b \quad (2.25)$$

$$F_{vca} = d_2 * \rho_w * g * (z + 10) * h_i * b \quad (2.26)$$

Theses calculations allow for the derivation of the specific cutting energy, the amount of energy required to cut or loosen $1m^3$ of soil. This equation comes out to be:

$$E = \frac{F_h * v_c}{h_i * b * v_c} \quad (2.27)$$

Dilatancy is the phenomenon by which the pore volume of a substance increases when a shear is applied. Before a shear is applied, particles settle into the smallest volume possible, but after shearing the particles lift and separate creating a decrease in the pore pressure. These forces are clearly dependent on whether or not the pore pressure has reached vapor pressure, at which point cavitation forms. Equation 2.28 was developed to determine the point at which cavitation occurs :

$$\Omega_1 = \arcsin\left(\frac{d_1 * (z+10) * k_m}{c_1 * v_{cir} * \cos(\iota) * h_{i\max} * \cos(\xi) * e}\right) \tag{2.28}$$

At the point of cavitation the forces are at a maximum since the pore pressure reach a constant with any additional cutting velocity. Miedema (1987) developed several equations to determine the cutting force coefficients c_1,c_2,d_1,and d_2.

$$c_1 = \frac{\left(p_{1m} * \frac{\sin(\varphi)}{\sin(\beta)} + p_{2m} * \frac{h_b}{h_i} * \frac{\sin(\alpha+\beta+\varphi)}{\sin(\alpha)}\right) * \sin(\alpha+\delta)}{\sin(\alpha+\beta+\delta+\varphi)} - p_{2m}\frac{h_b}{h_i} + p_{3m}\frac{h_b}{h_i} \tag{2.29}$$

$$c_2 = \frac{\left(p_{1m} * \frac{\sin(\varphi)}{\sin(\beta)} + p_{2m} * \frac{h_b}{h_i} * \frac{\sin(\alpha+\beta+\varphi)}{\sin(\alpha)}\right) * \cos(\alpha+\delta)}{\sin(\alpha+\beta+\delta+\varphi)} - p_{2m}\frac{h_b\cos(\alpha)}{h_i\sin(\alpha)} + p_{3m}\frac{h_b\cos(\alpha)}{h_i\sin(\alpha)} \tag{2.30}$$

$$d_1 = \frac{\left(\frac{\sin(\varphi)}{\sin(\beta)} + \frac{h_b}{h_i} * \frac{\sin(\alpha+\beta+\varphi)}{\sin(\alpha)}\right) * \sin(\alpha+\delta)}{\sin(\alpha+\beta+\delta+\varphi)} - \frac{h_b}{h_i} + p_{3m}\frac{h_b}{h_i} \tag{2.31}$$

$$d_2 = \frac{\left(\frac{\sin(\varphi)}{\sin(\beta)} + \frac{h_b}{h_i} * \frac{\sin(\alpha+\beta+\varphi)}{\sin(\alpha)}\right) * \cos(\alpha+\delta)}{\sin(\alpha+\beta+\delta+\varphi)} - \frac{h_b\cos(\alpha)}{h_i\sin(\alpha)} + p_{3m}\frac{h_b\cos(\alpha)}{h_i\sin(\alpha)} \tag{2.32}$$

These equations are functions of the angle of internal friction ϕ, the blade height h_b, the cutting thickness h_i, the pore pressures at different locations along the blade p_{nm}, the blade cutting angle α, the soil/interface friction angle δ, and the shearing angle β. An analogy to electrical resistors allows for the calculation of these pressures.

The following equations determine the pore pressure:

$$s_1 = (L_{\max} - L) * \cos(\theta_1) * \frac{\pi}{2} + (L_{\max} - L) * \sin(\theta_1) + \frac{h_b}{\sin(\alpha)} \tag{2.33}$$

$$s_2 = L * \theta_2 \tag{2.34}$$

$$s_3 = L * \theta_3 \tag{2.35}$$

$$s_4 = (L_{\max} - L) * \theta_4 + 0.1 * h_i * \pi \tag{2.36}$$

$$\begin{aligned} \theta_1 &= \frac{\pi}{2} - \alpha - \beta \\ \theta_2 &= \alpha + \beta \\ \theta_3 &= \pi - \beta \\ \theta_4 &= \pi + \beta \end{aligned} \tag{2.37}$$

The resistances of each line can be represented by the following equations:

$$R_i = \frac{s_i}{k_{\max}} \quad for\ i = 1, 2, 3, 4 \tag{2.38}$$

The total resistance is calculated by treating the resistors as a parallel circuit. In other words:

$$\frac{1}{R_t} = \sum_1^n \frac{1}{R_n} \tag{2.39}$$

These resistances allow for the calculation of the pore vacuum pressure at the shear zone. The vacuum pressure is the pressure at which the forces are the maximum due to the fact that cavitation occurs past this point. The value for the pore pressure:

$$\Delta p = \rho_w * g * v_c * e * \sin(\beta) * R_t \tag{2.40}$$

The vacuum pressure is then calculated across the shear zone. To calculate this pressure Miedema(1987) integrates numerically along the shear zone with the formula:

$$p_{1m} = \frac{1}{n}\sum_{i=0}^{n} \Delta p_i \ with\ l_i = i * \frac{L}{n} \tag{2.41}$$

A different method is employed to calculate the pore pressure along the side of the blade. To find this pressure the pore pressure is set to zero at the top of the blade. Assuming a linear profile from this starting point gives an average value of half the blade edge pore pressure. However, a linear pore pressure does not fit the curve properly. Applying a factor of f gives the following formula:

$$p_{2m} = \frac{\Delta p_n}{2} * f \tag{2.42}$$

$$f = \left(\frac{h_i}{h_b}\right)^{\pi/2 - 1.2*\alpha} * \frac{\sin(\alpha+\beta)*\sin(\alpha)}{\sin(\beta)} \tag{2.43}$$

Figure 3 demonstrates the increase in pore pressure that occurs during shearing. The first drawing shows the sediment particles in their unsheared state(with very little pore volume). The second picture demonstrates the great increase in pore volume that occurs during shearing, leading to a pressure change in each pore.

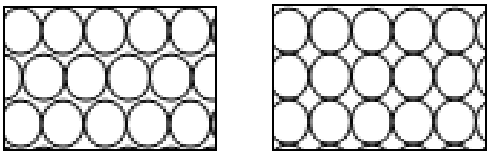

Figure 3. Dilitancy During Shearing

Miedema (1987) further developed the previous theory to apply the theory to an actual three-dimensional cutterhead. The resulting equations for one blade of the cutterhead are as follows:

$$F_a = -F_h * \sin(\iota)\cos(\xi) - F_v \sin(\xi) \tag{2.44}$$

$$F_s = F_h \cos(\iota)\cos(\Omega) \pm (-F_h \sin(\iota)\sin(\xi) + F_v \cos(\xi)) * \sin(\Omega) \tag{2.45}$$

$$F_v = \pm F_h \cos(\iota)\sin(\Omega) - (-F_h * \sin(\iota)\sin(\xi) + F_v \cos(\xi))\cos(\Omega) \tag{2.46}$$

$$M = F_h * \cos(\iota) * R \tag{2.47}$$

The angles iota(ι) and xi (ξ) adjust for the varying shape of the cutterhead. To determine the average cutting force on the cutter over time the instantaneous forces are integrated with respect to the angle covered by each blade and multiplied by the number of blades p.

$$F_{ct} = \frac{p}{2\pi} * \int_0^{\Omega_0} F_c * d\Omega \tag{2.48}$$

The effects of the shape of the cutterhead and the coefficients c_1,c_2,d_1,and d_2 are combined into six new coefficients to simplify operations. These coefficients are defined by:

$$g_1 = c_1 * \cos(\iota) * \cos(\xi) \tag{2.49}$$

$$g_2 = -c_1 * \sin(\iota) * \sin(\xi) * \cos(\xi) + c_2 * \cos^2(\xi) \tag{2.50}$$

$$g_3 = d_1 \tag{2.51}$$

$$g_4 = -d_1 * \tan(\iota) * \sin(\xi) + d_2 * \frac{\cos(\xi)}{\cos(\iota)} \tag{2.52}$$

$$g_5 = c_1 * \sin(\iota) * \cos^2(\xi) + c_2 \sin(\xi) * \cos(\xi) \tag{2.53}$$

$$g_6 = d_1 * \tan(\iota) * \cos(\xi) + d_2 * \frac{\sin(\xi)}{\cos(\iota)} \tag{2.54}$$

Additional coefficients were developed that take into account the location of any cavitation occurring on the cutter blade. These equations are based upon the shape of the cutter head and are listed below:

$$f_1 = \frac{\sin^3(\Omega_1)}{3} \tag{2.55}$$

$$f_2 = \frac{\cos^3(\Omega_1)}{3} - \cos(\Omega_1) + 2/3 \tag{2.56}$$

$$f_3 = \frac{\sin^2(\Omega_0) - \sin^2(\Omega_1)}{2} \tag{2.57}$$

$$f_4 = \frac{\Omega_0 - \Omega_1}{2} - \left(\frac{\sin(2 - \Omega_0) - \sin(2 - \Omega_1)}{4} \right) \tag{2.58}$$

$$f_5 = \frac{\sin(2 - \Omega_1)}{4} \tag{2.59}$$

$$f_6 = \cos(\Omega_1) - \cos(\Omega_0) \tag{2.60}$$

Using these equations gives results of:

$$F_{st} = c_{nc} * [f_1 * g_1 \pm f_2 * g_2] + c_{ca} * [f_3 * g_3 \pm f_4 * g_4] \tag{2.61}$$

$$F_{vt} = c_{nc} * [\pm f_2 * g_1 - f_1 * g_2] + c_{ca} * [\pm f_4 * g_3 - f_3 * g_4] \quad (2.62)$$

$$F_{at} = -c_{nc} * f_5 * g_5 - c_{ca} * f_6 * g \quad (2.63)$$

$$M_t = c_{nc} * f_5 * g_1 * R + c_{ca} * f_6 * g_3 * R \quad (2.64)$$

$$\text{with } c_{nc} = \frac{p}{2\pi} * \rho_w * g * b_{pr} * v_{cir} * h_{i\max}^2 * \frac{e}{k_m} \quad (2.65)$$

$$c_{ca} = \frac{p}{2\pi} * \rho_w * g * b_{pr} * (z + 10) * h_{i\max} \quad (2.66)$$

To verify any results from the cutting theory, it becomes necessary to physically measure the forces occurring on a cutter head during operation. The work of Glover (2004) allows for the modeling of a cutter suction dredge at the Haynes Coastal Engineering Laboratory. Glover (2004) developed the design for the current dredge modeling facility at the Texas A&M Haynes Laboratory. To scale the dredge carriage different measures were applied to find the similitude of the scale model within the laboratory. A major portion of his work was determining how to scale the sediment to be comparable to a model. Additionally, Glover (2004) developed the initial design of the dredge carriage load cells, which were intended to determine the loading upon the cutter suction head. The work done by Glover (2004) developed the foundation for the building and future operation of the dredge carriage. The basic free body diagram of the initial dredge carriage is shown in the Figure 4.

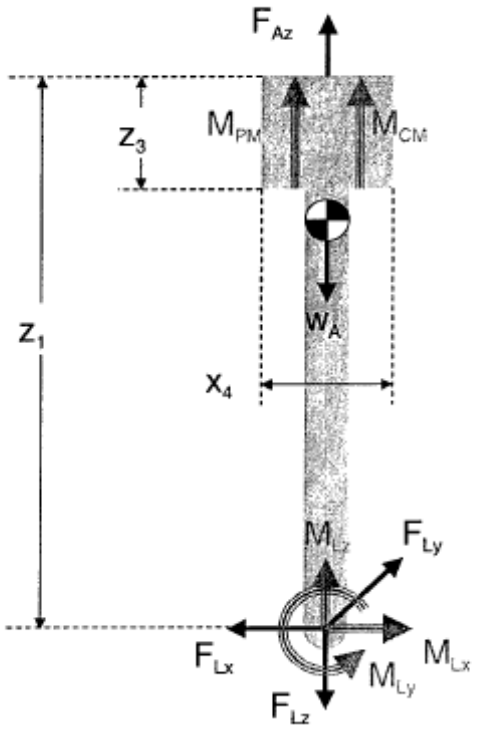

Figure 4. Free Body Diagram of Dredge Carriage (Glover 2002)

To measure the forces on the head of the cutter suction dredge model in the Haynes Coastal Engineering Laboratory, a system of load cells was installed to measure any forces the carriage experiences. Through the use of statics, the force on the cutter head is calculated based on the forces measured by the load cells. Young (2009) designed a model of the dredge carriage with SolidWorks to determine the best possible location for all the load cells.

To determine the accuracy of these readings a known load was applied to the cutter head and the theoretical forces for each load cell was determined by the

SolidWorks code. During the course of this testing it was discovered that the carriage was binding due to excessive force in certain situations. Due to this binding the load cells were not reading properly and it became necessary to install an additional load cell to absorb the load causing the binding. Once this was completed the system was tested once again for an applied load, and this time the results were more accurate. Load cell #1 is located at the top of the dredge carriage. The location of cell #2 is on the upper south side of the ladder cradle, cell #3 is located on the upper south-east corner of the cradle oriented in the east-west direction of the load cells and cell #4 is located on the opposite side of cell # 2 in the north to south direction. The sixth and final load cell is located on the lower southwest corner oriented from the north to the south. The dredge carriage used in these experiments now allows for the direct measurement of the forces on a cutter head for forces up to 0.889 kN (200 lbs).

A MATLAB program was constructed to calculate the forces on the cutterhead based on the readings of the load cells. The sensors were calibrated with a device designed by Young(2009) to determine their accuracy and the equations needed for the MATLAB program. Using these calibration equations statics was applied to solve the equations of motion on the cutter head. The completion of this program allowed for the collection of data during dredging operations. Since the dredge carriage is assumed to be a model of an actual dredge scaling laws can be applied to scale up the forces on the dredge and other aspects of the dredge cycle.

CHAPTER III

EXPERIMENT PROCEDURE

This thesis applies the cutter force theory developed by Miedema (1987) to the cutter suction dredge operated in the Haynes Laboratory. Once theoretical calculations are made, the dredge carriage is run for a variety of circumstances and comparisons are made between the two data sets. Ideally, the data sets match completely, but a good correlation allows for further tweaking of the theory to fit the specific cutter head. The end result is MATLAB program to estimate the average forces on a cutter head due to cutter velocity, sand type and other independent variables.

Laboratory Testing Procedure

The dredge carriage can be operated in both manual mode and remotely. In Figure 5 below the manual controls are shown. The ladder depth joystick is on the far left and the angle of the articulating arm is the next switch. The cutter speed is the next switch and the next joystick controls the motion of the carriage. The emergency off button is on the far right. Figure 6 shows the dredge carriage with all the critical parts of the carriage listed with arrows.

Figure 5. Picture of Manual Dredge Controls

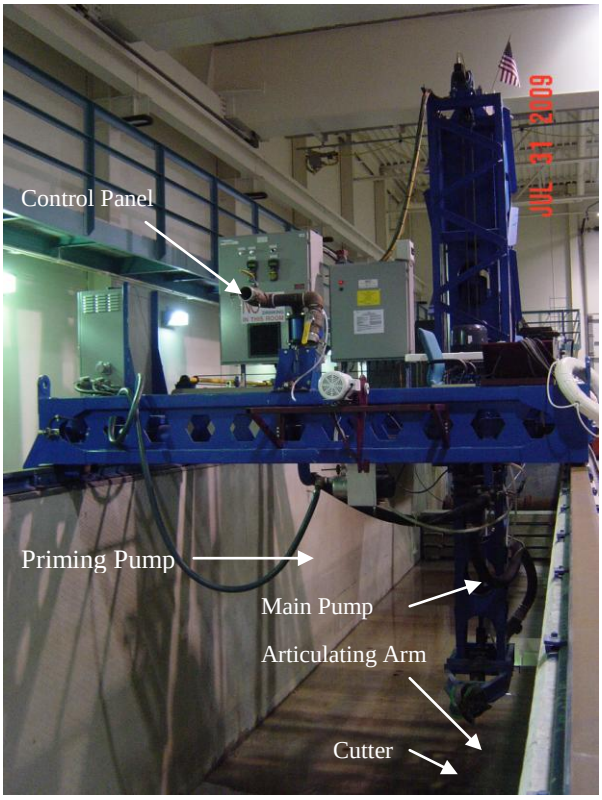

Figure 6. Model Dredge Carriage in Haynes Laboratory at Texas A&M University

The testing was performed to provide data for comparison to the computer program based on the theory. The testing varied the cutter RPM, the depth of the cut, the flowrate, and whether overcutting or undercutting was occurring. The main dredge pump required priming each time before starting. The line to the back of the smaller cooling pump was filled with water and dropped into the tank while the cooling pump was started. After the cooling pump was primed the main pump was primed using the cooling pump. After the main pump was primed the cutter head was started using the keypads on the data acquisition system. The carriage was operated with the manual controls to make a full cut. Each cut was started from the north to the south side of the pit which results in initial overcutting. The cutter was advanced east into the sediment and then to the north to begin undercutting. The dredging procedure consisted of lowering the cutter into the sediment bank and dredging the required amount of sediment from the pit. The sediment was cut in 4 (0.10 m), 6 (0.15 m), and 8 inch (0.20 m) deep cuts. To determine the depth of the cutterhead, the forces on the load cell above the carriage were observed for any changes that would indicate the presence of the bottom on the load cell that carried the largest amount of the ladder's weight. The depth of each cut was measured from these points. During each tests the data from all six load cells were measured in addition to the pressure sensors, the specific gravity, and the flowrate. During dredging the flowrate was monitored to ensure that the sediment was not settling within the pipe to the sand separator. The measurements from the load cells were taken and the forces on the cutterhead were determined using a modification of the program developed by Young (2009). During the testing procedure the water level was kept at approximately 2.5

meters(8.2 ft) from the top of the sand. The water depth partially determines the pressure experienced on the cutterhead. The last major parameter of the dredging process was the measurement of the angle of the articulating arm on the dredge. The angle of the arm was kept at either 30 or 35 degrees throughout the course of dredging depending on the depth of the cut being made. The angle of the arm influences the forces experienced by the cutter dramatically. Additionally, the RPM of the cutter drive was kept constant for each run. The RPM determines the amount of sediment suspended, and the forcing on the blades due to undercutting or overcutting. The program used for capturing data was written in Labview. The data were captured at a rate of 1 Hz for the duration of testing. The majority of the data used in this thesis was taken on February 5, 2010. The parameters for each test are listed in Table 1 with the rpm as the first column, the flowrate in gallons per minute as the second column, and the depth of cut in inches as the third column. Several of the test conditions were repeated to confirm initial observations.

Table 1. Experiment Parameters

5-Feb-10			
Test Case	RPM	Flowrate (GPM)	Depth of Cut(Inches)
1	29	250	4
2	43.5	250	4
3	43.5	250	6
4	29	250	8
5	43.5	250	8
6	29	250	6
7	43.5	250	6
8	29	250	8
9	43.5	250	8

Production During Dredging

The dredge carriage was operated at fairly high specific gravities throughout the experiment process that led to a large production rate. The production during dredging does not seem to have any significant effect on the cutting forces. The only possibility of increasing forces due to increased production is the chance of the depth of the cut increasing both the production and the forcing on the cutter. The limiting factor in production at the Haynes Laboratory is the dewatering system, which can process approximately 2.62 m^3 (2.0yd^3) of dry sand per hour.

Geotechnical Testing

Since cutting forces vary greatly with respect to the various types of soil, the sediment used in the tank was analyzed to determine the density, the porosity, the permeability, and the soil internal friction angle. In addition to these tests, the angle of steel/sand friction was determined by using estimates based on the internal friction

angle. The internal friction angle was determined by a direct shear test. The direct shear test consisted of applying a series of different pressures upon the upper surface of a sediment sample and then gradually shearing each sample until failure of the soil occurs. Using Mohr's circle the shear envelope can be determined which leads the angle of internal friction. Figure 7 shows the calculation of the Mohr-Coulomb envelope.

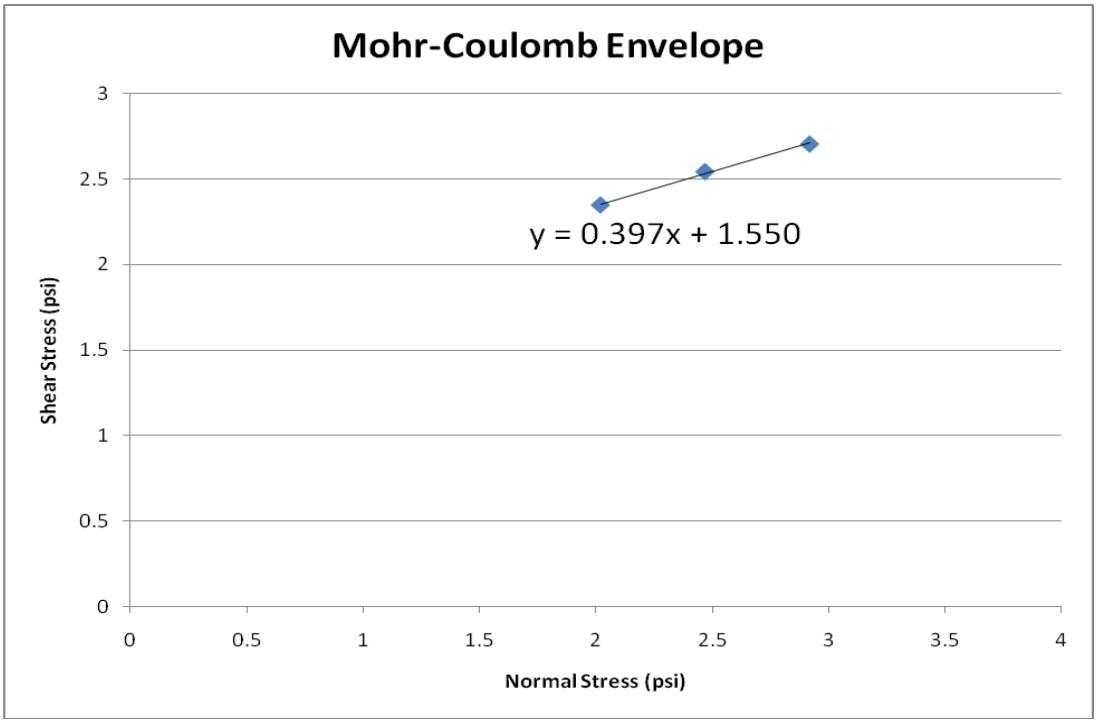

Figure 7. Mohr-Coulomb Envelope

The Mohr coulomb envelope determines the amount shear stress τ_f required for failure. The envelope can be approximated by a linear equation relating the cohesion ©, the normal stress on the failure plane σ, along with the angle of internal friction (φ).

$$\tau_f = c + \sigma \tan \varphi \qquad (3.1)$$

Using a simple linear regression within Excel allows for the calculation of the angle of internal friction by taking the arctangent of the slope of the line. The amount of cohesion of the sediment can also be determined, but in this case it is assumed that the sand is a non-cohesive sediment.

Figure 8 demonstrates the readings taken to determine the shear stress for three different normal stresses. Shearing occurs at the point at which the curve levels off.

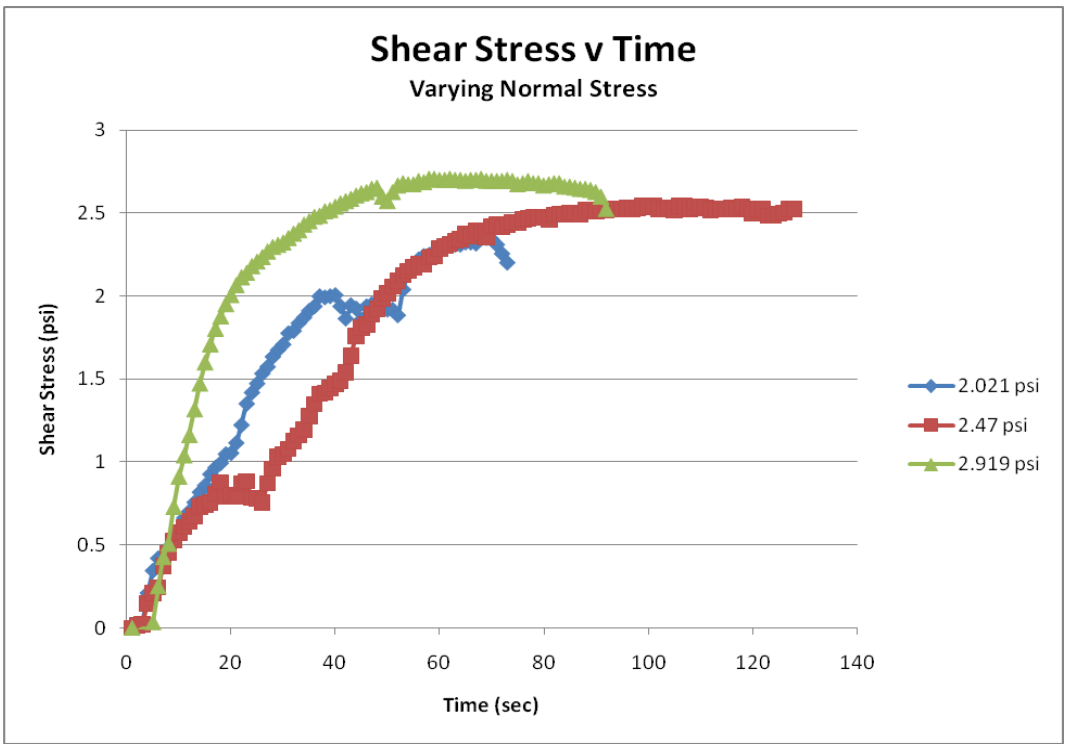

Figure 8. Plot of Shear Stress

The point of failure for the sediment occurs at the peak of the shear stress during the direct shear testing. Once the shear applied hits the breaking stress, the sediment shears

and lessens in resistance. These peaks are selected manually in excel and then plotted in the previous plot to determine the value for the angle of internal friction. The amount of force applied to compress the sediment was varied to get differing points.

In addition to the direct shear test the grain size was determined for the sediment used. The standard sieve test was used to size the sand, and the results led to a d_{50} of 0.28 mm sand. The measured grain size allows for a quick check to see if the values for the sand/steel friction coefficient compare to past results. The results of the sieve test are shown in Figure 9.

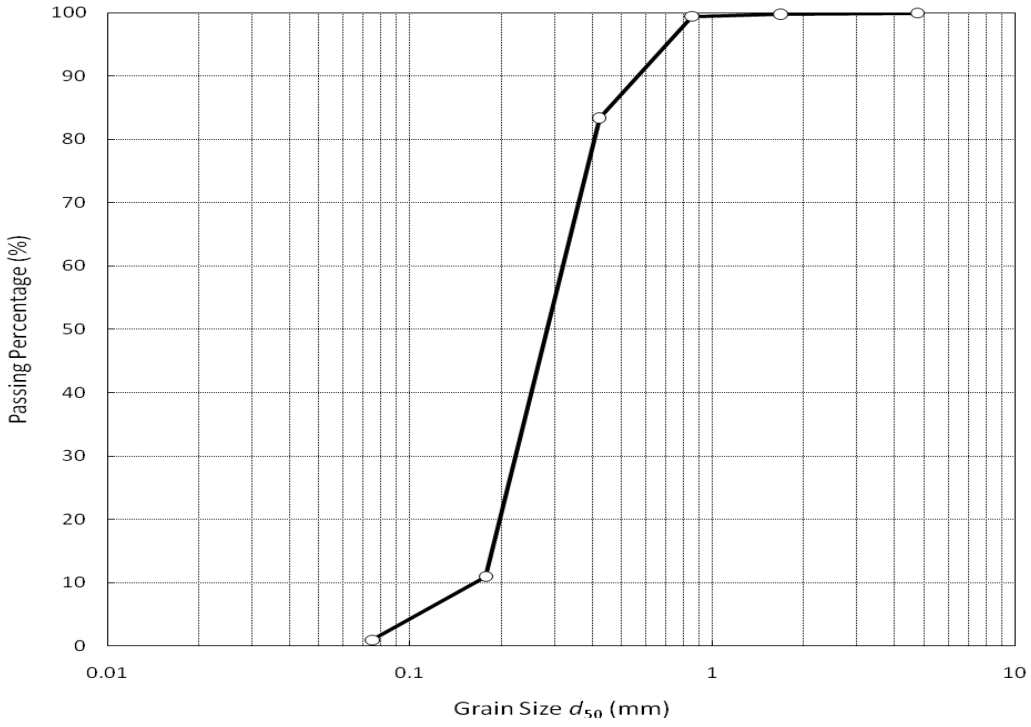

Figure 9. Sieve Test Results

The final geotechnical test performed was the constant-head permeability test. This test is performed using a cylinder filled with the sediment being tested with a continual flow of water through the top of the cylinder. The water flows through the sediment and out a spigot in the bottom of the apparatus. The pressure of the inflow is kept constant due to the use of a small reservoir of water kept at a constant depth through the use of a hole at the required level. The resulting flow was timed by stopwatch and measured using a beaker. The average flowrate for the sediment used was 0.00048 m/s. Using the formula for permeability with the constant-head test:

$$k = \frac{QL}{Aht} \tag{3.2}$$

gives the result of 0.000419 m/s for the sediment in the current configuration.

MATLAB Program Procedure

For the MATLAB code to estimate the value of the forces on the cutterhead, the cutting theory was applied to the dredge carriage in the Haynes Coastal Engineering Laboratory. Several different MATLAB functions were introduced determine each component of the force equations and to allow for easier debugging. Each function dealt with a piece of the puzzle in the theory. To determine the theoretical forces using prior work, it became necessary to determine many of the parameters in his equation. The cutting force depends on quite a large number of variables.

Dimensions of the Cutter Blade

The blade on the cutter was positioned at angle of 30 or 35 degrees with respect to the horizontal. Therefore, the angle alpha was set to the angle corresponding to the angle at which the articulating arm was set at the time. Each blade is also offset from the

axis of the cutter at an angle ι. The blades are each offset from the axis of the cutterhead by the angle ξ. These angles are critical for the influence of the cutter shape. The cutter head being used on the dredge carriage has a more tapered shape than those used by Miedema(1987), and this greatly influences the overall results on the forcing of the cutter. IN ORDER TO determine these angles, a digital protractor was employed. The blade width is about 11cm and the blade projected area is determined by:

$$b_{pr} = b * \cos(\iota) * \cos(\xi)$$

This equation determines the area of the blade that will experience forcing during dredging. Measuring the height of the blade on the cutter and multiplying by the sine of the angle of the articulating arm, determined the height of the blade (h_b). Using a height of 26 cm and a ladder arm angle of 35° gives the value for h_b = 14.913 cm. Additionally the radius of the cutterhead was measured at R=0.18 cm.

Depth and Thickness of Cut

The depth of cut was assumed to be constant throughout the dredging cycle. The depth was symbolized by B_υ. The thickness of the layer cut by the dredge is determined by a simple formula:

$$h_i = h_{i\max} * \sin(\Omega_0) * \cos(\xi) \tag{3.3}$$

$$h_{i\max} = \frac{v_s * 60}{n_o * p} \tag{3.4}$$

In the previous formulas p stands for the number of blades, n_o is the RPM of the cutterhead, 0.025 m/s (v_s =1.0 inch/s) is the haulage velocity (the velocity across the

tank), and Ω is the angle being covered by the cutterhead. In this case it is assumed that Ω is determined by the formula:

$$\Omega_0 = \arccos(1 - \frac{B_v}{R}) \tag{3.5}$$

In the previous formula R is the radius of the cutterhead and B_v is the breach height, or the depth of the cut.

Soil Properties

To determine the permeability of the soil the standard geotechnical test outlined above was applied. The permeability of the soil resulted in a value of approximately k= 0.00106inch/s (0.000419 m/s). This value compares favorably with other results for sand in the past. To determine the sand steel angle of friction it became necessary to determine the angle of internal friction of the soil.

Calculating Porosity

Porosity plays an important part in calculating the forces on the cutter blade. The porosity determines the pore pressure and influences the effects of dilitancy on the substance. Porosity is defined by the ratio of the volume of voids to the total volume, or n. The porosity is also related to the volume strain by the following ratio:

$$e = \frac{n_{\max} - n_i}{1 - n_{\max}} \tag{3.6}$$

The porosity for the sand used in the experiments in the Haynes Laboratory was estimated using the average values for sand. The value used for the theoretical forces for

e=. n_{max} and n_i were not necessary for the sand in question since the values for n_{max} and n_i were used to determine e.

Conversion of Axis Systems

To convert the results to the Cartesian coordinates that have been the basis for all the work of Young (2009) it is necessary to apply several trigonometric identities. In the Miedema (1987) theory, the axes are defined as along the axis of the ladder(a-axis), perpendicular to the axis of the ladder vertically(s-axis), and tangent to the motion of the cutter(vaxis). These coordinates are shown in Figure 10 and Figure 11. Young (2009) applied Cartesian coordinates to the forces on the dredge carriage in the Haynes Coastal Lab. The main reason for these discrepancies is the difference in the way each dredge operates. The dredge in the Haynes Coastal Engineering Laboratory operates on a track in a straight line as opposed to an arc, the natural path of a cutter suction dredge operating with spuds. The axis systems were converted within the code to determine the forces based on Miedema's theory. The necessary equations are listed below:

$$F_x = \cos(\alpha) * F_a - \cos(90 - \alpha) * F_s \tag{3.7}$$

$$F_y = F_s \tag{3.8}$$

$$F_z = \sin(\alpha) * F_a + \sin(90 - \alpha) * F_s \tag{3.9}$$

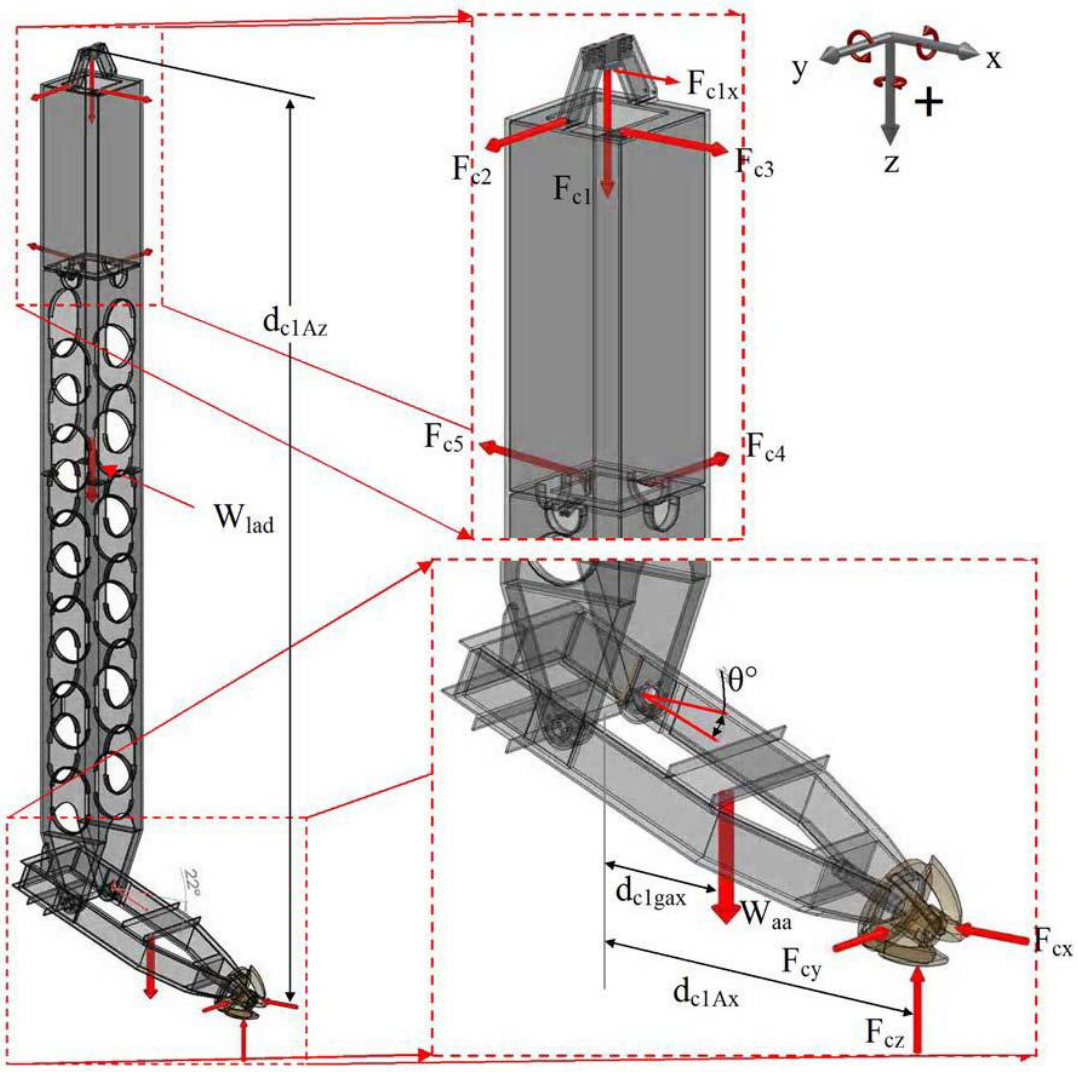

Figure 10. Definition of Axis System (Young 2009)

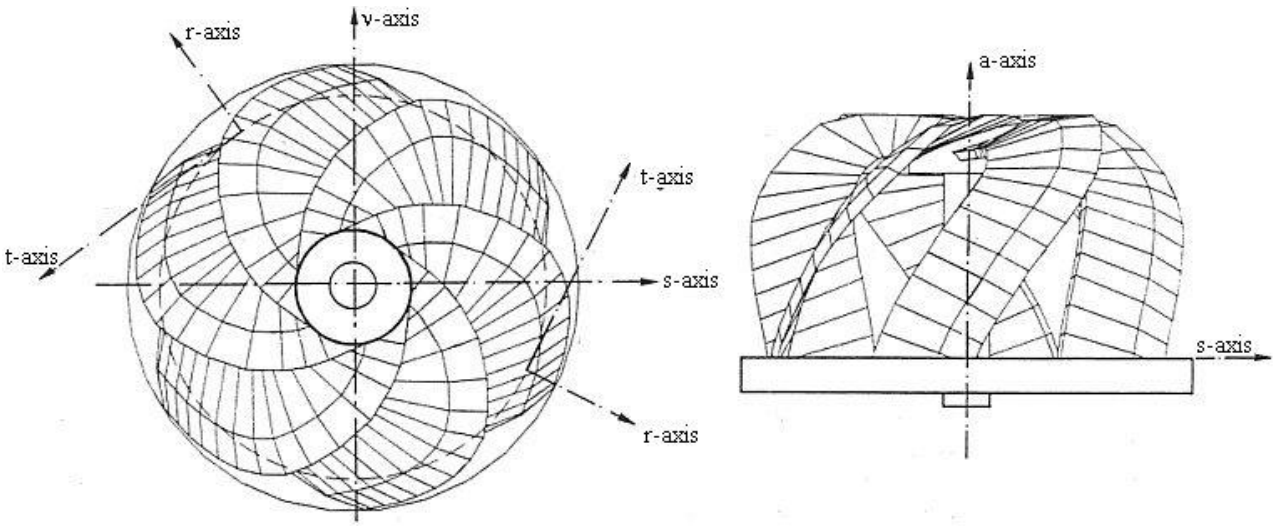

Figure 11. Definition of Axis System (Miedema 1987)

Determination of Shear Angle

To determine β(the shear angle), an estimation was made using a plot developed by Miedema (1987) work. For a blade angle α=35 the angle β=30 seems to be the correct choice for the shear angle. The angle can also be determined by applying the Newton-Raphson method, but for the purposes herein the interpolation will suffice. Figure 12 shown below allows for the determination of the angle by setting the partial derivative of the forces equal to zero and determining the point of intersection with the plot of the forces. The angle at this point is used for the shear angle.

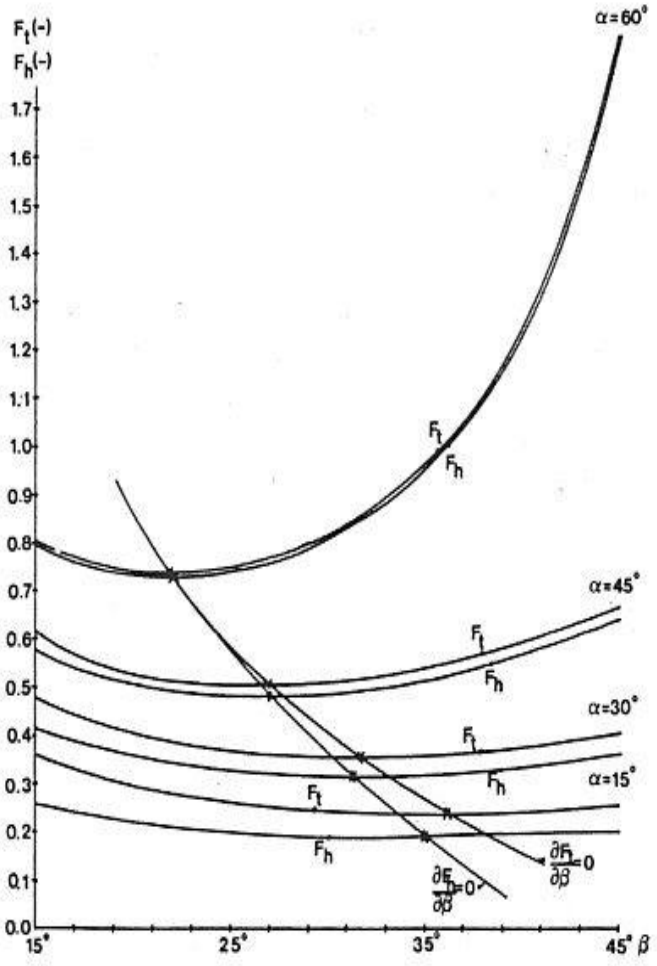

Figure 12. Plot of F_h vs. β (Miedema 1987)

Determination of Blade Cutting Angle

The angle α was the easiest parameter to determine on the dredge carriage since it is simply the angle at which the ladder arm is facing. For the tests performed on February 5 the angle was set at a constant value of 35 degrees. For the dredge carriage, the ladder angle (α) plays a large role in the ability of the cutter to reach the sediment

without being embedded into the sediment bank. In previous studies, the ladder arm has scraped the bottom causing some inconsistencies within the measurements.

Cutter Speed

The cutter speed controller was set at a maximum of 290 RPM and was operated at speeds of 10% and 15%, which leads to n_o to be 29 RPM and 43.5 RPM respectively. The cutter is powered by an electric motor whose maximum speed is 1740 rpm. This motor is then geared down by a 1:6 ratio to a maximum speed of 290 RPM. These speeds are more than capable of providing the sediment required to operate the dredge at full production.

Program Scheme

The program used to determine the theoretical forces was performed using several different subprograms to calculate various parts of the theory. Each of these programs is called in the main program to determine the forces for either undercutting or overcutting. A diagram of the program scheme is shown in Figure 13. The advantage of these programs is in debugging and adjusting for various parameters in the theory.

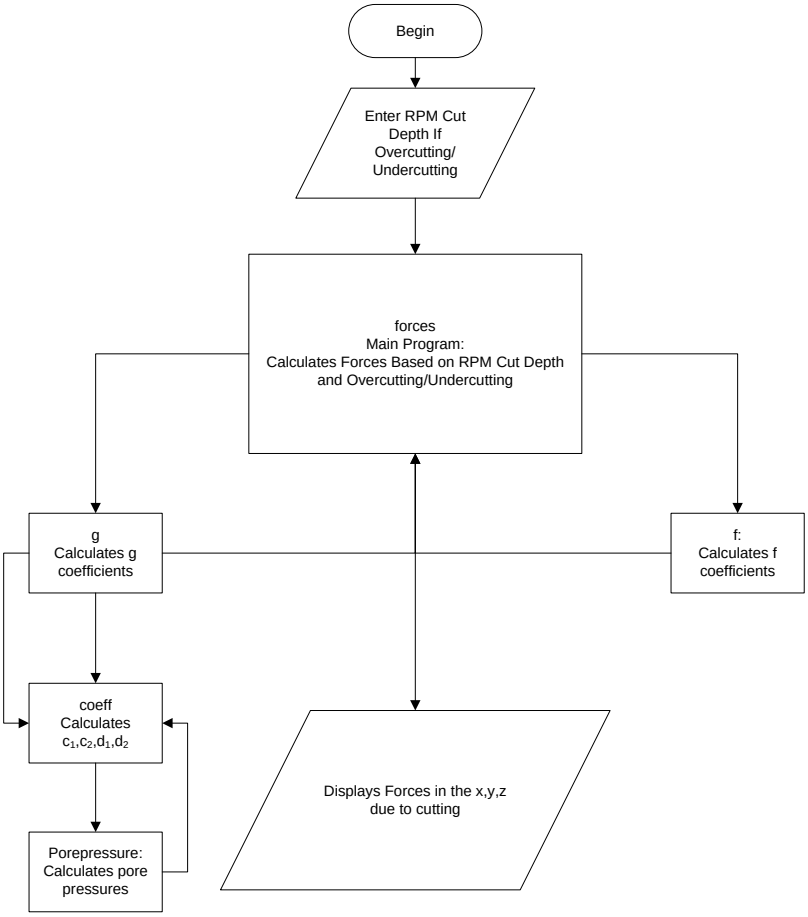

Figure 13. Diagram of Theoretical Program

Theoretical Force Calculations

This is the main program involved in calculation of the forces according to theory. The inputs are the cut depth, the RPM of the cutter drive, and whether or not the cutter is overcutting for the cut being performed. This program allows for the estimation of forces in all scenarios used in the testing performed on February 5. The program then calls two other programs to calculate the coefficients.

Forcing Coefficient Calculations

This subprogram calculates $f_{1\text{-}6}$ by applying the formulas given previously. The formula is based on Ω_1 and Ω_0. g calculates $g_{1\text{-}6}$ based on the values of c_1, d_1, c_2,and d_2. These values are calculated using the equations listed above. The program calls the function coeff to calculate the necessary coefficients and then imputes the values of c_1, d_1, c_2,and d_2 as well as ξ and ι into the equations for $g_{1\text{-}6}$.

Cavitating and Noncavitating Coefficient Subprogram

This subprogram calculates the values of c_1, d_1, c_2,and d_2 by using the equations based on the various geometries of the cutterhead and the sediment. To calculate the pore pressures necessary the subprogram modified from the resistor theory was called to determine the coefficients.

Program to Determine Pore Pressure

To calculate the coefficients necessary to apply theory a subprogram to execute the resistor theory was created to determine pore pressure. The program uses the theory of resistors as an analog to the actual behavior of the pore pressures in such a circumstance. The pore pressure is a factor of many different variables dealing with the blade. The other option to calculate the pore pressures underneath the blade uses a finite element model To model the pressure field around the cutterhead. This method gives slightly better results but is much more computationally expensive.

CHAPTER IV

ENGINEERING FACILITY

The Haynes Coastal Engineering Laboratory provides a great opportunity to study the forces on a cutter suction dredge and allows for the measurement of the cutter forces through a different method than previously established. The Haynes Laboratory was constructed from August 2001 to June 2003. The lab has multiple capabilities with a shallow water wave basin and a dredge/tow flume. Both the shallow water wave basin and the dredge tank allow for the development of a current of up to 132,000 liters per minute(35,000 GPM) when necessary. The wave basin can generate virtually multiple wave spectra, and allows for a wide array of coastal studies. This research uses the facilities developed in the Haynes Laboratory to measure the forces on a cutterhead directly through the scale model of a cutter suction dredge. The previous work by Young(2009) and Glover(2004) has provided the necessary equipment and software to determine the forces on the cutter at any given moment in time. The forces are measured by the force transducers and logged using a data acquisition system written in Labview.

Tow Tank

The tow tank dimensions are 45.6 m(150 ft) long by 3.66 m(12 ft) wide with a sediment pit 7.56 m(24.8 ft) in length and 1.52 m(5 ft) deep. The overall dimensions of the tow tank are shown in Figure 14 in English units. The sediment pit allows for various studies involving not only dredging, but also any study directly related to processes on the ocean floor. The maximum water level of the tank is 3.04 m(10 ft).

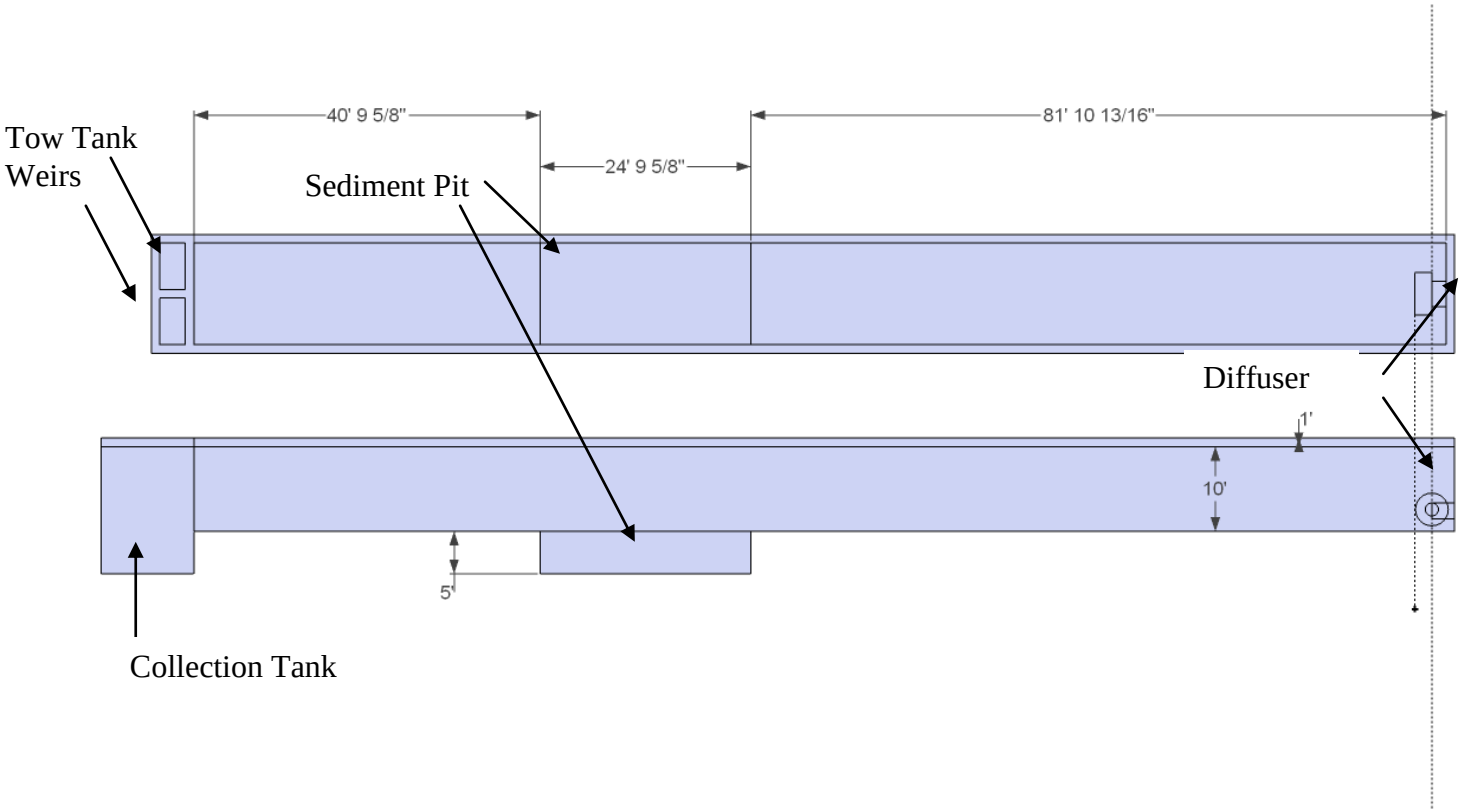

Figure 14. Tow Tank Diagram

To develop a current in the tow tank a water diffuser is located on the west side of the tank that can generate up to 132,000 liters per minute (35,000 GPM) for testing. To collect the water two weirs are located on the east side of the tow tanks that can empty the tank in a short period. The tank also has several observation windows (located both above the sediment pit and within the sediment pit) for video and instrumentation. In clean sand the dredging process can be easily observed.

In Figure 15 the main pump is being primed. A small pump primes the main with water drawn from the tow tank. The main pump is then started with all valves on the back of the dredge closed. Once the pressure in front of the valve builds up the valves are slowly opened until the pump is running steadily.

Figure 15. Dredge Carriage in Operation

Dredge Carriage

The initial design criteria was developed by Glover (2002), and is shown in Figure 15. The final design was implemented by DACS(Digital Automation and Control Systems) and Oilfield Electric Marine. In addition to the dredge carriage, a dewatering system is installed at the west end of the dredge carriage. The sand/water separation system allows for the capture of sediment for reuse in later projects. The system consists of two hydrocyclones and a pair of elliptical pattern vibrators, which are used as shale shakers in the oilfield. The hydrocyclones are shown at the upper right hand side of the Figure 16, and the two vibrators are painted white. The slurry mixture enters the vibrator on the left and is filtered through a coarse sieve that removes any large particles in the sediment. The resulting slurry is then pumped through the pair of hydrocyclones that separate the majority of the slurry from the water and the finest sediments. That mixture is then placed on the finer sieve on the right that sorts most of the sand out of the slurry. Figure 16 demonstrates the use of the system to remove silt from sediment dredged during the study.

Figure 16. Sand Separation System in Operation

The dredge carriage is mounted on top of two rails and is driven by a pair of electric motors. The dredge pump is a four inch suction, three inch discharge slurry pump capable of pumping at specific gravities as high as 1.7. The carriage also has a nuclear density meter and a flow meter, which allows for the calculation of production. The articulating arm on the ladder can operate at angles from 0 to 50 degrees. During this research, the angle was alternated between 30 and 35 degrees depending on the depth of cut needed. To get a deeper cut, it was necessary to dredge directly in front of the intended cut to avoid scraping the sediment with the articulating arm. Several sensors

are in place to monitor the carriage in all directions and prevent collisions. The capabilities of the dredge are shown in Figure 17.

Category	Design Requirement
Velocity	Tow carriage must achieve 1.2 m/s (4 ft/s) during towing operation
Acceleration	Tow carriage must accelerate from 0 to 1.2 m/s (4 ft/s) over 12 m (40 ft)
Weight	Removable dredge carriage limited to 2721 kg (6000 lb)
Weight	tow carriage and dredge carriage not to exceed 4534 kg (10,000 lb) total
Force	Max side-winch pull force not to exceed 3559 N (800 lb)
Cutter Power	14.9 kW (20 hp)
Pump Power	7.46 kW (10 hp)
Side Winch Power	2.24 kW (3 hp) each side
Flow Rate	Maximum 1893 LPM (500 GPM) from 7.62 cm (3 in) pump
Control System	Automated and manual operation
Data Acquisition	Real-time display and data storage
Digging Depth	3.05 - 4.27 m (10 - 14 ft) measured from the cutterhead axis leaving 178 mm (7 in) clearance to tank bottom
Swing Travel	1.6 m (63 in) on either side of center measured from the cutterhead axis leaving 229 mm (9 in) clearance to each side of tank
Ladder Angle	0 to 90 degrees from horizontal
Discharge	Not to interfere with dredging operation

Figure 17. Dredge Capabilities (Glover 2002)

The dredge cradle was powered by a 1.1 kW motor for both the side-to-side and vertical ladder motion. A pair of 3.8 kW motors drive the carriage motion up and down the tracks. The ladder slides back and forth on two horizontal cylinders that lay across the cradle. The lower ladder angle is limited to 50 degrees to the horizontal due to binding on the universal joint. The cutter head on the carriage is a five bladed model that has a radius of about 18 cm (7.1 inches) and a height of about 26 cm (10 inches). Photographs of the cutterhead used in the studies at the Haynes Laboratory are shown in Figure 18.

Figure 18. Cutter Head Used in Haynes Lab

Data Acquisition System

A program in Labview was written to read the forces produced by the cutter head on the six transducers. In addition to the forces on the transducers the specific gravity and the flow rate were measured to determine the effects of the flowrate on the forces on the cutter. These measurements also allow for the calculation of the production rate during the dredging. The data acquisition software was used to record data at a rate of up to 10 Hz. During this study a 1 Hz sampling rate was used since most dredging processes occur at a slower rate.

Force Transducers

The load cells used on the dredge carriage are 13.3kn (3000lb) gauges. These gauges have an accuracy of 0.25%, which is 0.033 kN (7.5 lbs) for the maximum loading. The safe overload is 20 kN (4500lbs) and the ultimate overload is 40 kN (9000lbs). The calibration procedure on the force transducers initially consisted of an apparatus constructed by Young to compress the transducers to measure the readings for each transducer and later progressed to a method in which the transducers could be calibrated without the removal of the transducers from the dredge carriage. The results of Young's (2009) calibration for the six load cells are listed in Figure 19 with the given equations. The result for the final load cell was retrieved following further testing on the load cell.

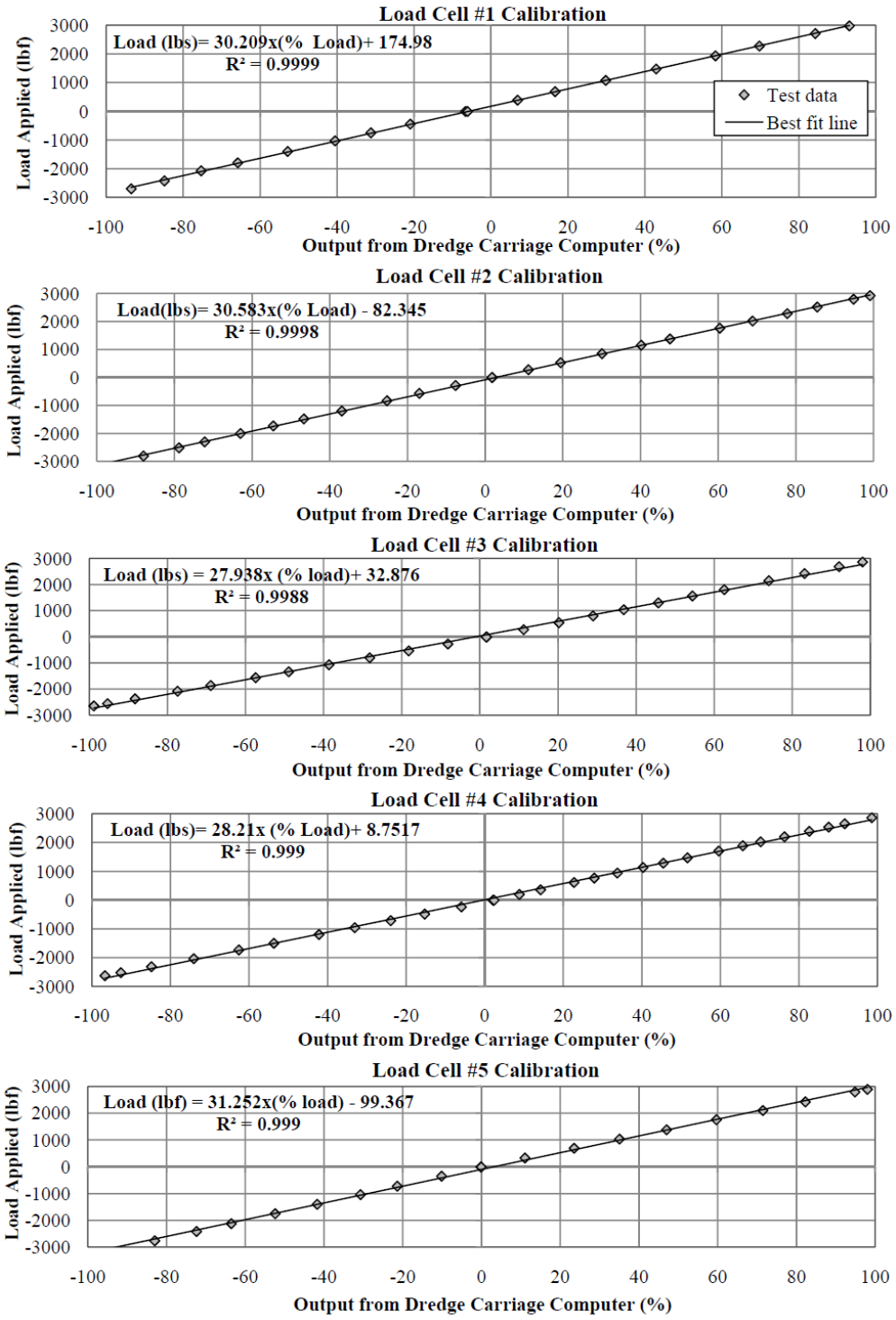

Figure 19. Calibration Equations for Load Cells

CHAPTER V

LABORATORY DREDGING RESULTS

The data were gathered from the dredging, and then the results from the program to calculate theory were compiled. To accommodate for the variability in theory the data for the dredging was time averaged for the undercutting and overcutting cases. The results being compared are from February 5, when the data was measured for three different depths of cut. The advantage to using data all within the same timeframe is that the sediment profile will be similar throughout this period. Additionally, the data was visually checked for outliers.

Dredging Results

The dredging results were compiled using a slightly modified version of the MATLAB code developed by Young (2009). The program outputs both the forces in the x, y, and z as well as three plots for each set of data. The plots show every jump in the force due to the variety of factors involved in the dredging. The program also allows for the calculation of the average forces on the cutter during both the undercutting and overcutting stages of the dredging. The average forces allow for good estimates of design forces toconstruct a cutterhead in the future. The code for the program is listed in Appendix A. The results fall within the plots of the measured experimental forces. For the first test in the Y direction, the theoretical force was 55 % less than the measured forcing for the overcutting stage of the experiment. The theoretical was 9.7% smaller in magnitude compared to the measured for the undercutting portion. However, the unevenness of the bottom was a concern. The large spikes seen are believed to be due to

the buildup material on the bars the ladder arm slides across. Plots of the forces in the x,y, and z directions were constructed for every test condition and show the forces experienced in each direction due to different dredging scenarios.

Forces in the Y direction

Figure 20 shows the results of the first test in the Y-Direction for a cut of about 6 inches. The forces vary widely, ranging from 800 N (180 lbs) to about -267 N (–60 lbs). The plot also shows significant peaks every 20 to 25 seconds indicating a low frequency forcing behind the steadier forcing due to the cutter interaction. The lower frequency forcing is believed to be due to the buildup of material between the collar of the ladder and the chrome bars they slide on.

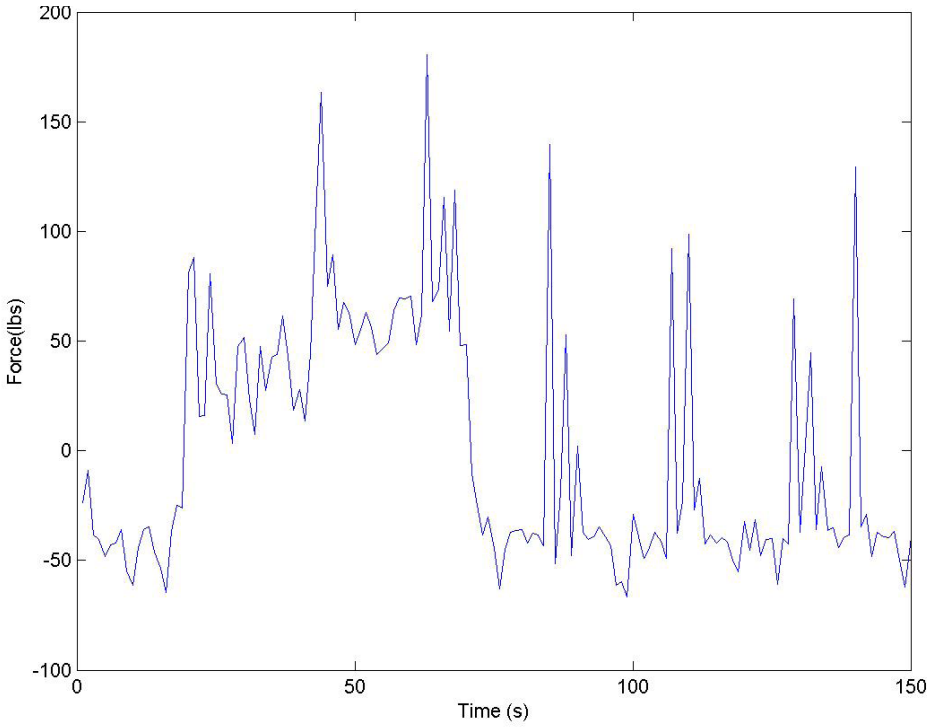

Figure 20. Forces in the Y Direction for Test 1

The average force for the first 75 seconds of measurement (overcutting) is 198 N (44.4 lbs) and the second half (undercutting) is about 194 N (43.1 lbs) in the negative direction. These forces seem slightly small, but the symmetry makes sense. Due to the slow motion of the cutter blade the majority of the force in the y-direction should come from the forces due to the blade biting into the sand. The change in direction from overcutting to undercutting explains the change in force from positive to negative over the course of the cut. The peaks during the dredging are a periodic forcing of the cutter due to buildup of material on the bars due to the wearing of the collars attaching the ladder of the dredge carriage to the carriage. Additionally the slight inertial effects caused by the buildup of sand on the cutterhead can cause some random data to occur. This occurs because of the occasional sandbank in the uneven bottom of the sediment pit.

During the testing shown in Figure 21 a clear spike occurs at 75 seconds (at which point the dredge is advancing). The force is due to the sudden increase in the sand bank that causes a large lateral forcing on the cutterhead as the untouched sediment is introduced. This force is similar to that experienced on an actual cutter suction dredge operating with a spud carriage. In a dredge that does not operate with a spud carriage the transition to the deeper sediment is much more gradual since the cutterhead is allowed to swing into the bank versus the spud carriage that advances directly into the sediment. The force seems to be best estimated by the use of some soil strength tests, as well as tests to determine the level of compaction of the soil in-situ.

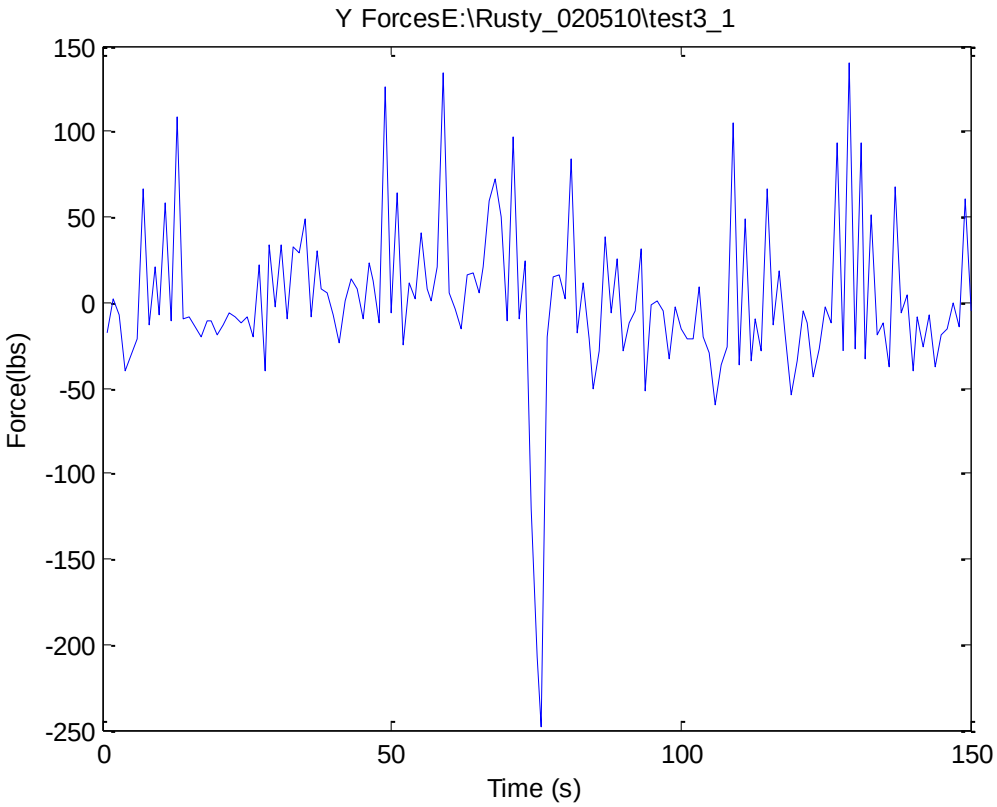

Figure 21. Forces in the Y for Test 3 (lbs)

Forces Compared to Slurry Specific Gravity

Figure 22 demonstrates the lack of correlation between the specific gravity of the slurry being dredged. The two plots are non-dimensionalized by their respected averages. The two factors would seemingly be correlated in that the deeper the cut the higher the forces on the cutterhead and the higher the specific gravity. The flowrate could also have a theoretical effect in that it might change the pore pressure surrounding the cutter head. If the flowrate was insufficiently removing the sediment surrounding the cutter, a bank of sand could develop in front of the face of the cutterhead causing higher

than normal forcing. However, if too much suction was applied the force the blade would experience as large a pressure gradient across the blade surface.

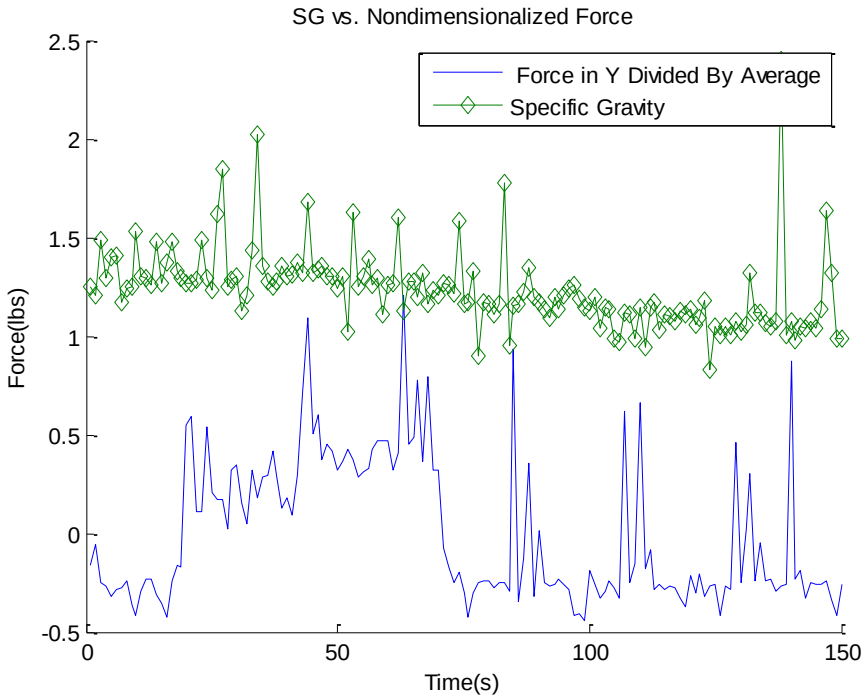

Figure 22. Nondimensionalized Force vs. Specific Gravity

Fast Fourier Transform of Force Measurements

To determine if the sampling rate was enough to capture the entire phenomenon taking place during the cutting process a fast fourier transform was performed for each testing direction with a sampling rate of 25 hertz. This led to a Nyquist frequency of 12.5 hertz for Figure 23. Theoretically, there should be a forcing that is very low frequency, which would lead to a large spike at 0 Hz. This spike is shown in the FFT graph for the X-forces. This justifies the sampling rate of 1 Hz for each of the other runs.. However

there are some spikes in the forcing at higher frequencies. These spikes are caused by the changes in the cutting forces due to the position of the blade in the cut. Upon initial impact of each blade into the soil the forcing in the given direction will spike. The forcing in the x direction seems to be the one least affected due to the periodic fluctuations due to the motion of the blade. This is intuitive since the forcing in the x direction is more due to the amount of embedment into the sand.

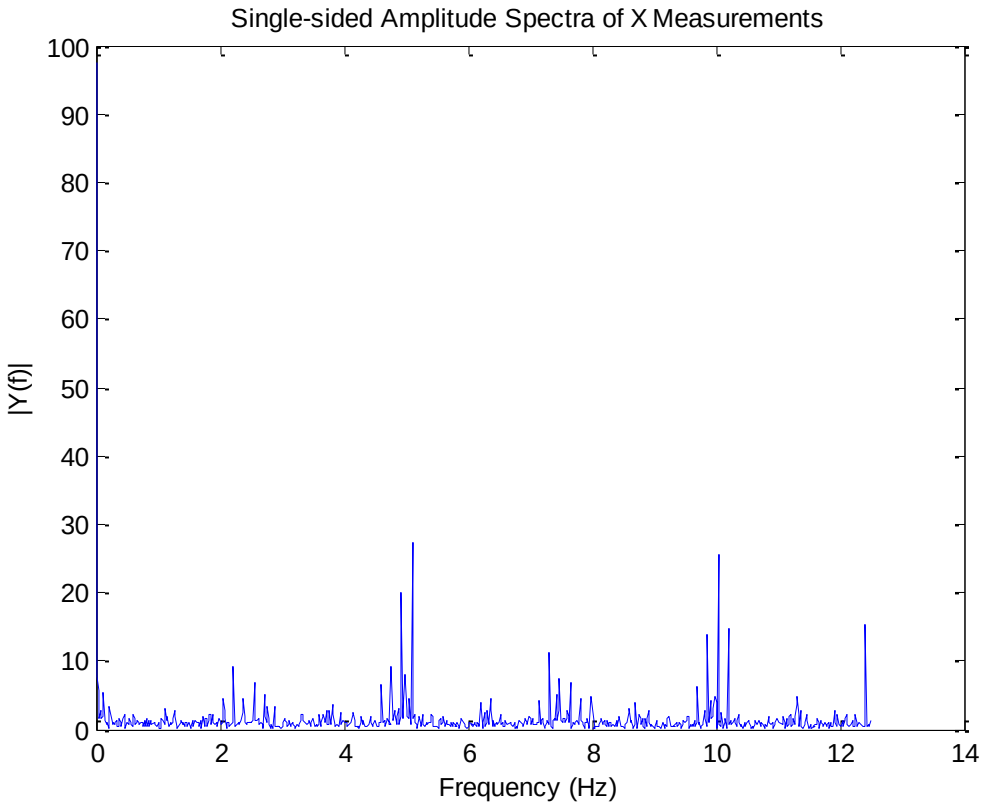

Figure 23. Fast Fourier Transform of X-Forces

Figure 24 shows the FFT of the forcing in the Y direction for the first test. The majority of the energy in the signal occurs at the lower frequencies. Once again, spikes

can be observed in the forcing at the frequencies of the cutter and the subsequent multiples of the cutting frequency.

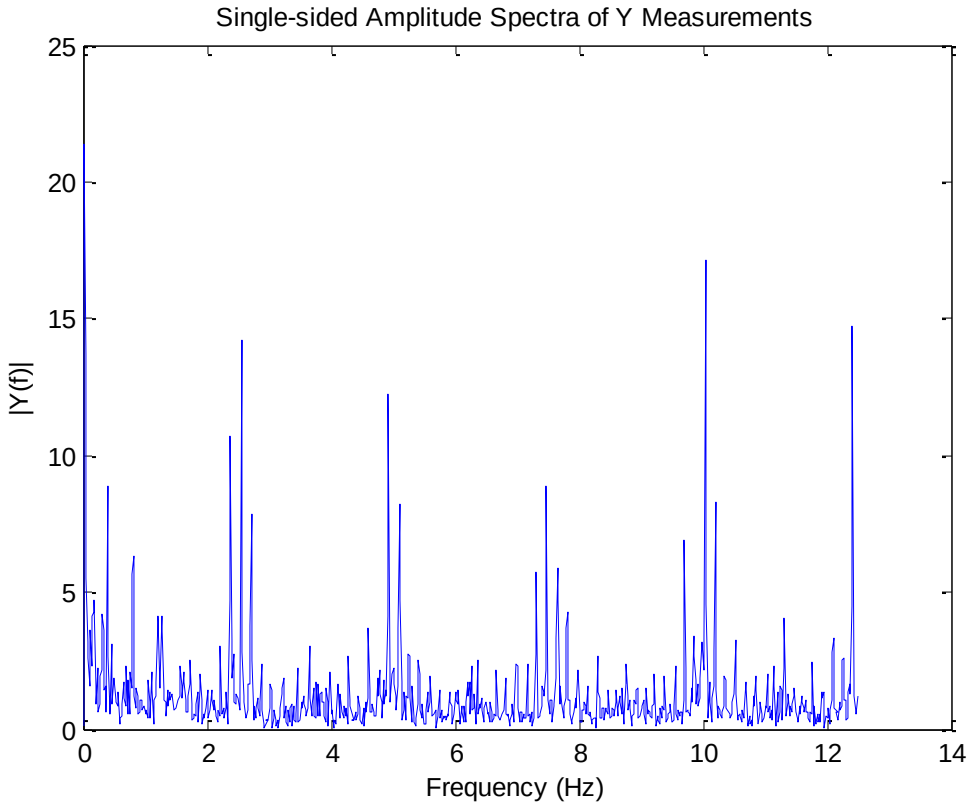

Figure 24. Fast Fourier Transform of Y-Forces

The z forcing seems to be affected the most by the higher frequency motion of the cutterhead. Figure 24 shows a lesser peak located at the lowest frequency with the largest peak located at 5 Hz. Figure 25 demonstrates that the major factor in the forcing in the z component of the experiment occurs with the initial contact of each blade with the sediment. The peak frequency for the z forcing is about 5 hertz.

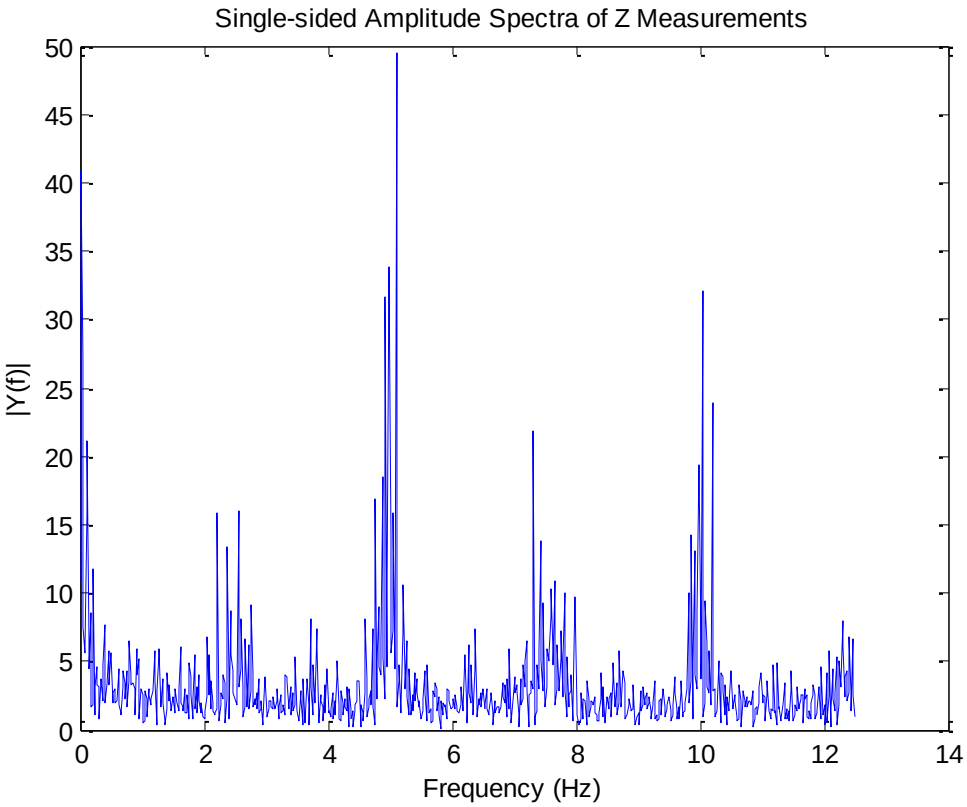

Figure 25. Fast Fourier Transform of Z-Forces

Forces in the X Direction

Figures 26 and 27 show the calculated forces developed using the equations of Young (2009). The plots are similar since the parameters for each test were kept constant. For these two tests the rpm was set to 43.5 and the cut depth was 8 inches. The forces for the first test ranges from -1110 N (-250 lbs) to 800 N (180 lbs) as shown in Figure 26,and the second test ranges from 890 N (-200 lbs) to 445 N (100 lbs) as shown in Figure 27.

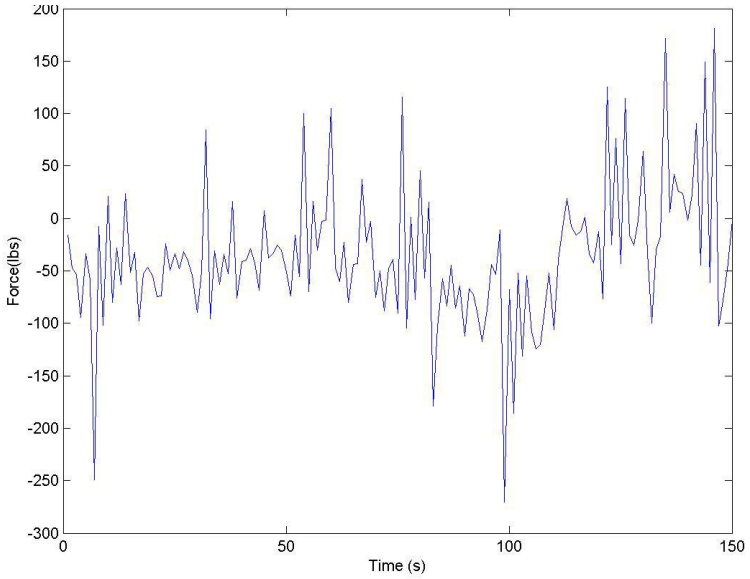

Figure 26. Forces in the X Direction for Test 5

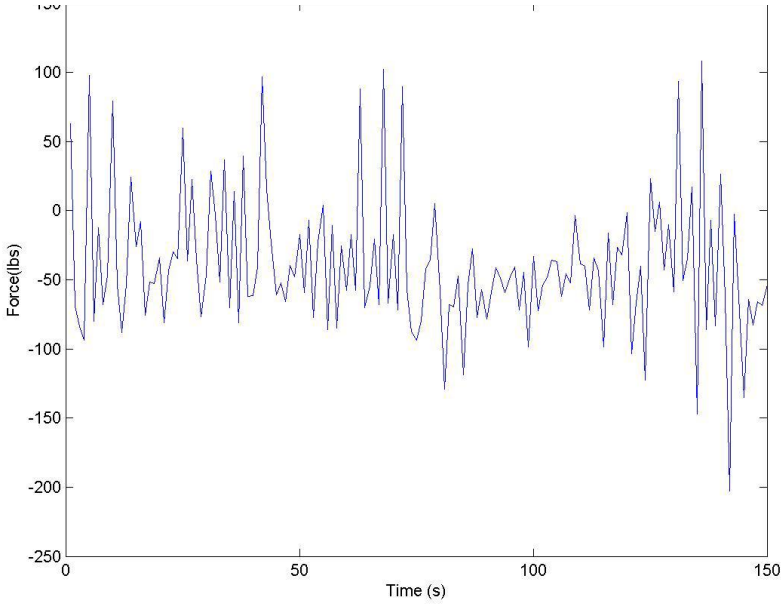

Figure 27. Forces in the X Direction for Test 9

These two tests show the variability that occurs during regular dredging operations. The topography along the seafloor or sediment pit of any dredge project is critical to determining the forces applied on the cutter. The sediment pit in the Haynes Laboratory had variations in depth. These variations are experienced by the cutterhead and are shown in the variations in the forces. The variations are also demonstrated in the averages of the respective forces. For test 5 the average x force for overcutting was 176 N (-39.5 lbs) and the result for undercutting was -147 N (-33.0 lbs). For test 9 these forces came out to be -27.7lbs(123 N) and -50.6 lbs(225 N) respectively. These forces indicate that the forcing on the x direction increased during overcutting in the first test and decreased with overcutting in the second test. Although the forces vary between these two tests the range of values covered are similar.

Forces in the Z Direction

Figure 28 shows the measured forces for the third test scenario. The forcing on the z for test 3 averages about 30.7 lbs (136 N) for the overcutting phase and about -50.7 lbs (226 N) for the second half of testing.

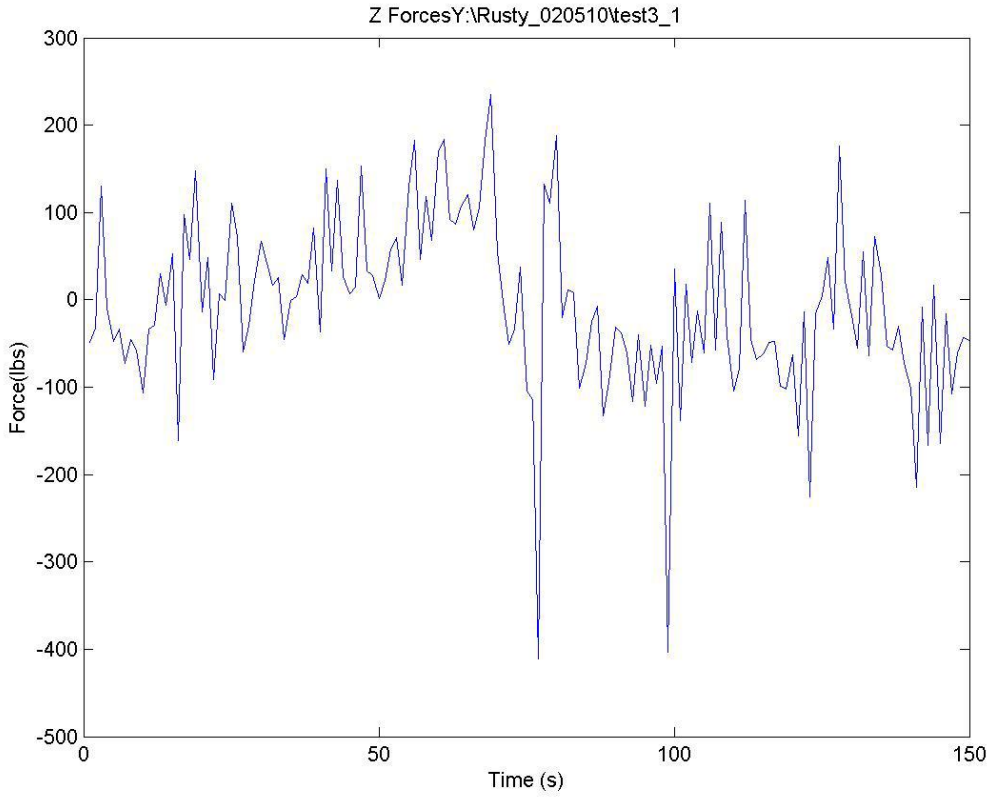

Figure 28. Forces in the Z Direction for Test 3

These forces seem slightly small compared to the peak forces being measured, but the averages seem correct. The peak shown is experienced during the advancing stage of the cut where the blade is beginning to undercut much of the new sediment. The spike occurs due to the impulse caused by the cutterhead impacting the newly cut sediment on the swing side of the cutterhead. The spike in force due to a forward

advance rather than a swing motion is the key factor in designing a cutter for a spud carriage alignment. The shift between overcutting and undercutting is also clear. The forces remain positive for the majority of the first half of the testing and shift negative in the second half of the testing. This is due to the cutter biting into the soil upon initial contact for overcutting. The majority of the force during undercutting results from the force caused due to the upward swing of the blade to shear the sediment. The sediment pushing back against the blade results in an overall negative forcing.

CHAPTER VI

RESULTS FROM CUTTING THEORY

The MATLAB results estimate the average theoretical cutting forces for the overcutting and undercutting processes. The forces are determined for each cut depth and cutter RPM. The force seems to match the measured averages closely, definitely close enough for design purposes. The plots in this chapter compare the measured forces with a plot of the average theoretical force.

Pore Pressure Results

The pore pressure was determined by the method of resistors described by Miedema (1987). The results of the theory were within 6% to that of Miedema and seemed to work well for the required problem. The pore pressures were a critical part of determining some coefficients. The pore pressure factors calculated compare favorably with those calculated by the use of finite element theory. The pore pressures calculated are vacuum pressures. Therefore, the magnitude of the vacuum pressure behind the blade increases with increasing RPM until it reaches a point at which cavitation occurs, the pore pressure reaches the vapor pressure of the water. At this point the vacuum pressure can't proceed any further so the forces (due to dilitancy) reach an asymptote. The pore pressures are fairly reasonable compared to the theoretical results. These pressures are an important part of determining the coefficients c_1, c_2, d_1, and d_2. In the future, a model of the cutterhead within a finite element method would be more effective in determining the value for each pore pressure.

Pore Pressures For Test Cases

The dimensionless pore pressures listed in Table 2 show the relationship between rpm and depth of cut for the testing performed on February 5. The two deeper cuts demonstrate the leveling off of the pore pressures at deeper depths and higher rpm since the values for both 6 inches and 8 inches at 43.5 rpm are the same. Another interesting aspect of is that the pressure remains constant whether or not the blade is overcutting or undercutting. The main equations address the issue by simple sign changes depending upon which type of cutting is occurring.

Table 2. Pore Pressures for Test Cases

Dimensionless Pore Pressures			
P1	P2	Depth (inches)	RPM
0.2792	0.008	4	29
0.2813	0.0057	4	43.5
0.2786	0.0087	6	29
0.2808	0.0062	6	43.5
0.2786	0.0087	8	29
0.2808	0.0062	8	43.5

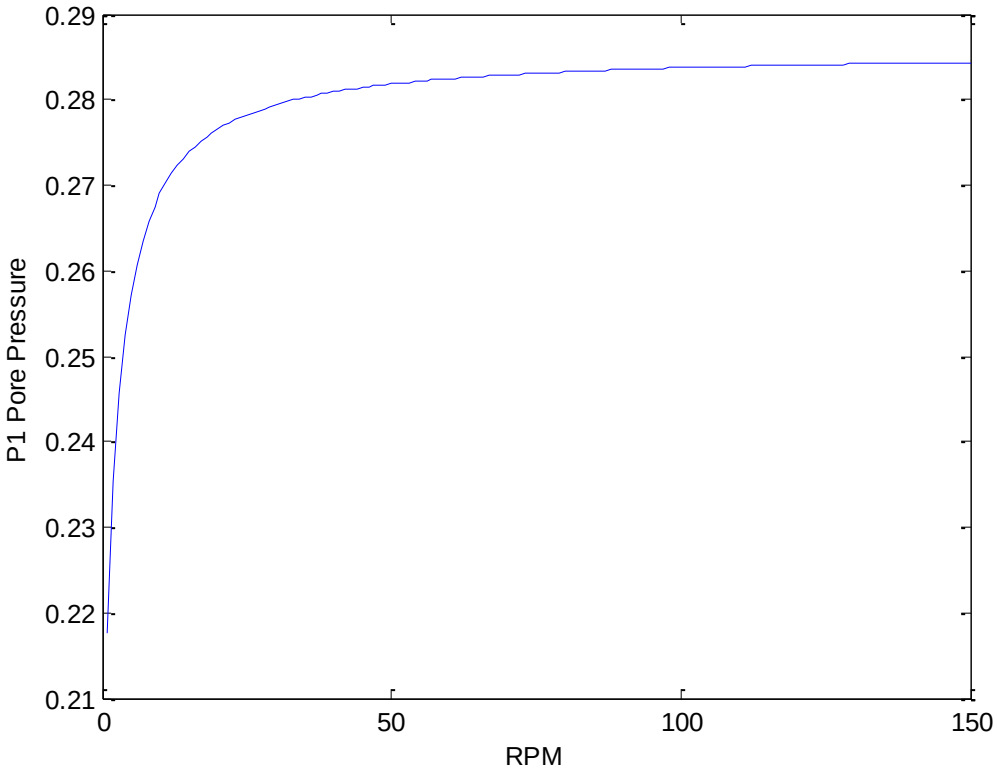

Figure 29. Comparison of Pore Pressures and RPM

The asymptotic behavior of the pore pressures in Figure 29 is an additional indicator of the lack of additional cutting force with higher cutter rpm. The forces on the cutter level off at much the same rate. The pore under pressure reaches a maximum when cavitation occurs. The rpm is one of the biggest variables when it comes to the pore pressure for a given scenario, especially since it is one of the parameters that can be regulated on a dredge. The pore pressure also varies very slightly with increasing depth of cut. The variation in pore pressure due to depth is fairly negligible in the experiments at the Haynes Laboratory since the majority of the pressure terms are generated solely by

the speed of rotation and not the pressure due to depth of cutting. The other variables used in resistor theory are constant for the experiments performed at the Haynes Laboratory. The difference in forces due to the depth of the cut is due primarily to the increased blade surface area exposed to the pressures with a larger cut. Figure 30 shows the relationship between pore pressure and cut depth. The pore pressure decreases steadily with increasing depth of cut. The decrease in pore pressure due to depth of cut is an outcome of resistors.

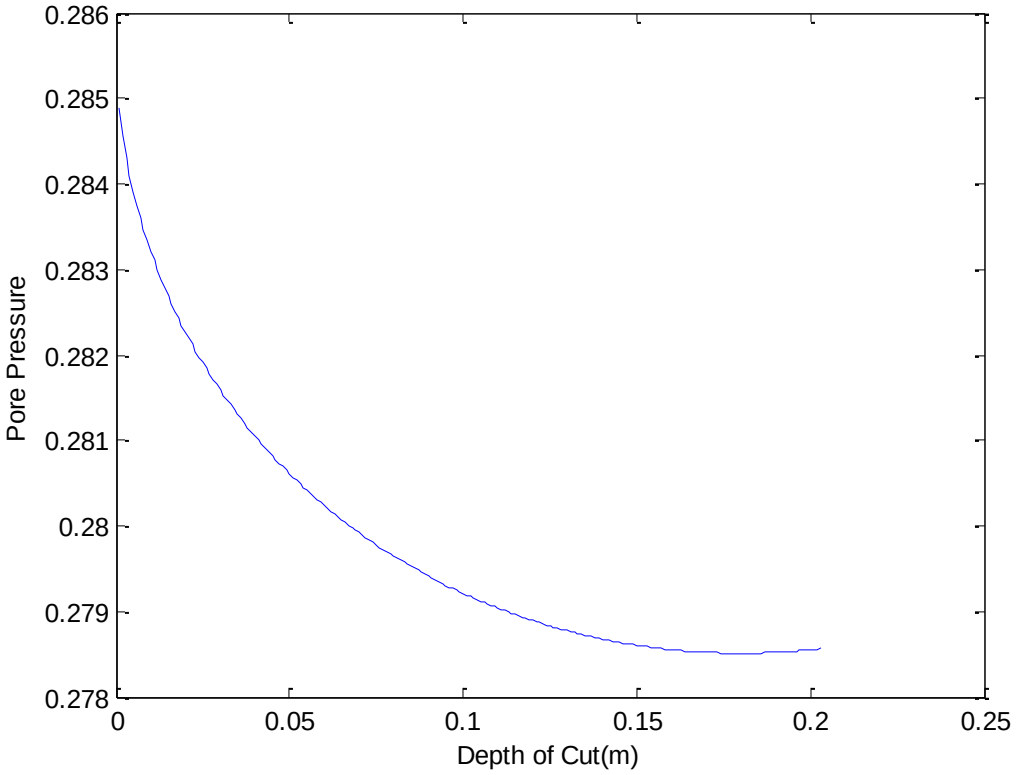

Figure 30. Comparison of Pore Pressures and Depth of Cut

Results for Forces

The results for the forces in each test condition are shown in Table 3. Each test condition used in the testing is shown in the table in both the undercutting and overcutting scenarios.

Table 3. Forces(lbs) for Test Cases

Overcutting X	Overcutting Y	Overcutting Z	Undercutting X	Undercutting Y	Undercutting Z	Speed	Depth
-33.95	19.076	23.4	-1.73	-39.36	-22.63	29 RPM	4 inches
-28.06	10.17	22.18	-3.35	-34.63	-13.12	43.5 RPM	4 inches
-43.17	19.82	44.44	13.91	-51.61	-37.07	29 RPM	6 inches
-36.56	6.62	39.89	7.65	-48.71	-23.25	43.5 RPM	6 inches
-55.11	14.76	67.73	31.56	-60.87	-56.04	29 RPM	8 inches
-46.4	21.5	58.4	20.9	-60.89	-37.72	43.5 RPM	8 inches

These forces show the ability of the theory to provide good estimates for the mid-range of the forces experienced by the cutter head at the Haynes Laboratory. The major factor in the force was the depth of the cut. The force in each direction increased fairly steadily with an increasing depth of cut. The forces are reasonable approximations for the average forcing on the cutterhead. For design purposes a factor of safety is necessary. The forces for the y direction are a little high for the undercutting case but the forces for the overcutting are about the right magnitude. The differences between the forces for different rpms are almost negligible, but the difference between the depths of cut is much larger.

Effects of Cutter RPM

The effects of the cutter rpm were observed using the force equations plotted for various rpm. Figure 31 demonstrates that the rpm does not greatly influence the forces past a certain value.

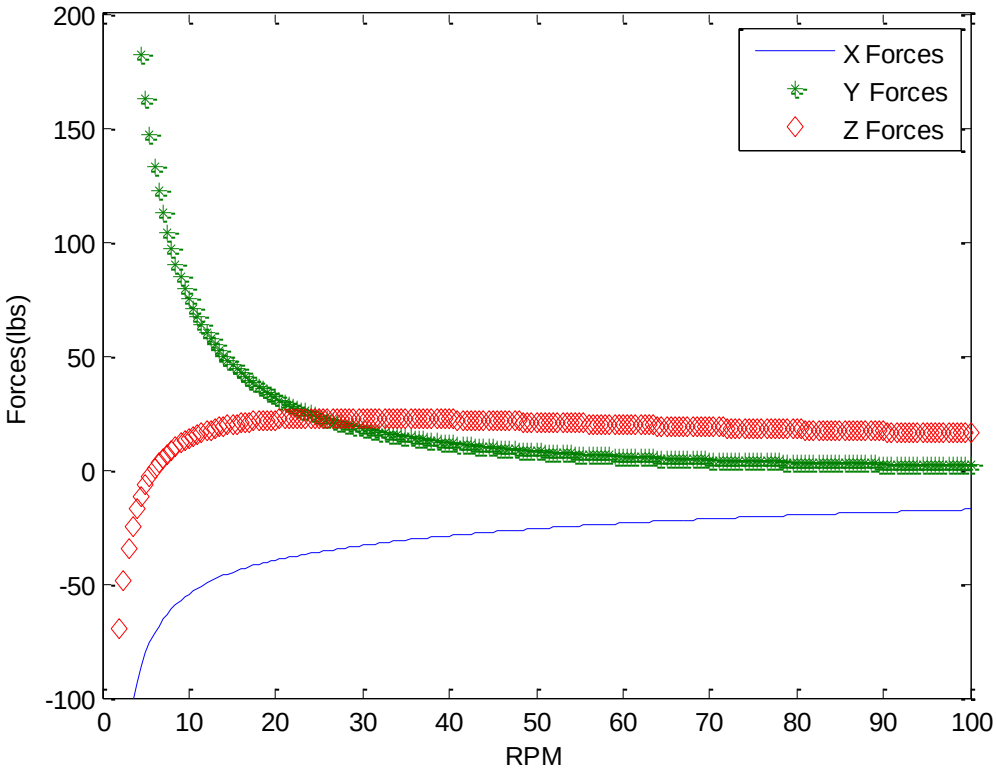

Figure 31. Effects of RPM on Theoretical Forces(Overcutting)

The reason behind this is that once the rpm reaches a speed sufficient to cut the material being introduced to the blade by the horizontal motion of the cutter, and any extra rpm are wasted in stirring up the sediment. Any additional rpm past the critical rpm only increases turbidity in the water and leads to less efficient dredging due to the

suspended sediment. Additionally, the size of the cut depends on the rpm of the blade. Every increase in angular velocity results in a decrease in the thickness of the cut. Once the rotative speed of the cutter reaches a certain velocity, the blade is basically shaving sand off of the sand bank. At some point the theory on cutter forces is no longer valid since inertial forces begin to take over from the dilitant forcing. Once the speed is reached the theory no longer applies. As far as practical application of this theory, the maximum production should be determined, and the rpm is adjusted to provide just enough sediment to maintain the production rate. The goal of the cutter is to supply the dredge with just enough sediment to maintain the desired specific gravity. The forces shown in the Figure 30 represent the mentioned effects. The rpm shown in the plot demonstrate the full range possible for the cutter assembly at the Haynes Laboratory. Any further increase in rpm is detrimental to the equipment at the laboratory and doesn't lead to any further increases in dredge production. The forces shown in Figure 31 were due to overcutting. Figure 32 shows the forces due to undercutting at 29 rpm for a cut of depth of 6 inches. The forces due to undercutting show similar reactions to variations in rpm to that of the overcutting process in that in both cases the force levels off significantly after a certain rpm. In Figure 31 (overcutting) the z forces are positive for most rpm. The force levels off fairly quickly in the plot due to the processes discussed earlier. The y forces start strongly positive at low rpm and eventually level out above zero for higher rpm. The forces are influenced by the larger cut necessary at smaller rpm which causes a positive force in the y. The x starts in the negative and comes back up towards zero before leveling out at –25 lbs (111 N). The reason for this is the lack of a

sediment bank for the blade to bite into and pull on the blade. The higher rpm does not allow the sediment to pull on the blade like the lower rpm. The plot for the forces due to undercutting in Figure 32 demonstrates the changes that take place between the two phases of dredging. The z forces are explained by the fact that the forces in the z direction are caused by the sand being undercut pushing down on the blade during undercutting. The forces are much larger in magnitude using lower rpm and become smaller as the angular velocity of the cutter increases. The y forces begin strongly negative and level out to about -40 lbs (178 N). The x forces begin higher but decline to about zero during higher rpm. The x forces are once again influenced by the lack of a significant sediment bank to create any forcing on the front edge of the blade. These forces both start high since the blade is cutting a larger amount of sediment at lower RPM and are lower due to the smaller layers of sediment cut at higher RPM.

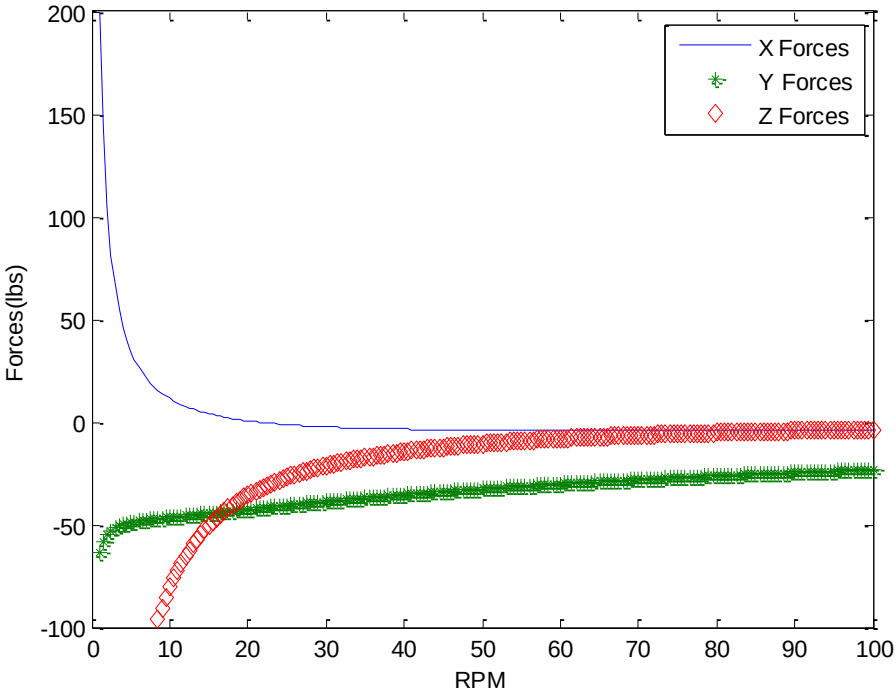

Figure 32. Effects of RPM on Theoretical Forces(Undercutting)

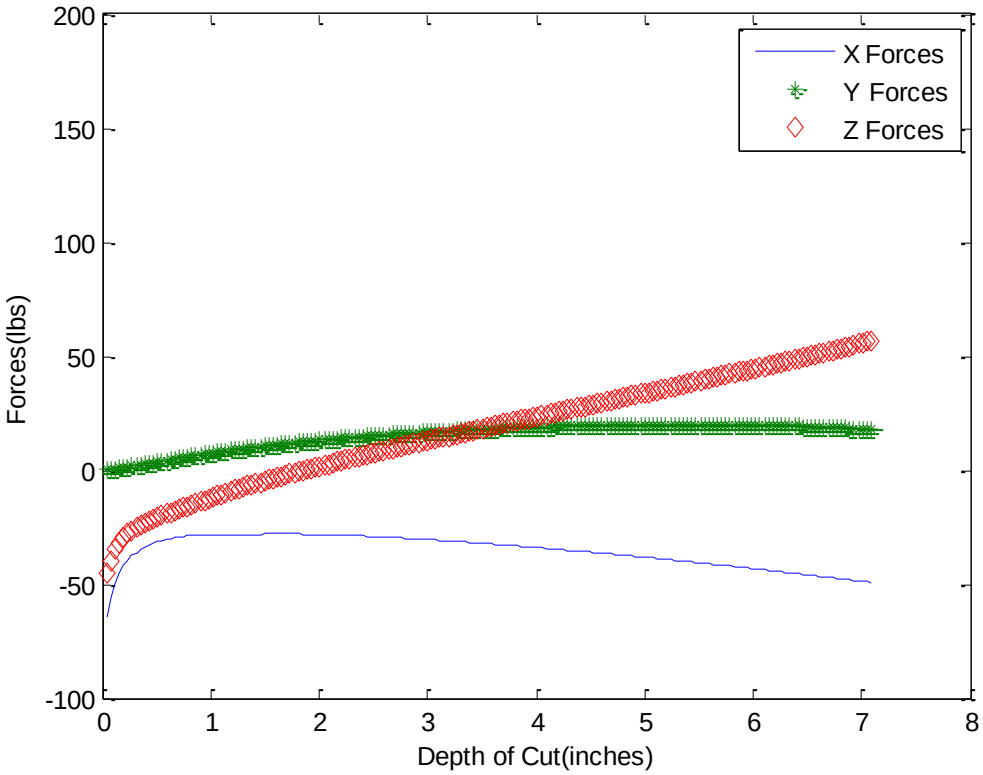

Figure 33. Effects of Cut Depth on Theoretical Forces (Overcutting)

The forces increase fairly steadily in magnitude in the z direction as the cut depth is increased. They seem anomalous for the first section of Figure 33. The force changes direction for the y component midway through the range of depths. This change in value is caused by the fact that for a deeper cut the initial impact of the cutter blades occurs at a continually higher point. This transfers the impact force applied by the blade initially penetrating to the z since with increasing cut depth the blade will eventually be cutting near perpendicular to the sediment. This phenomenon also leads to a steady increase in the z forces due to higher cut depths and the resulting transfer of forces. However, in the

case that the rpm is not sufficient to cut the material at the given swing rate the y forces may vary in a different manner. In the case that the rpm was too small for the swing speed, the force would change from one direction to the other as the front of the blades was jammed into the sediment bank. Figure 34 demonstrates the change in the forces due to undercutting. The forces display quite different behavior compared to overcutting. The forces in the z start negative and initially trend towards zero since for an extremely shallow cut the majority of the force in the z direction will be caused by the blade entering the sand and not the force needed to move the sand upward. Once the blade is embedded into the sediment deep enough to require the cutting of a sizeable sediment bank, the force to move the sand upward causes a negative force on the z since the blades will eventually leave the sediment at a perpendicular. The force in the y direction increases in magnitude fairly steadily with depth for undercutting since the initial impact of the blade will always occur in the y direction . This is due to the fact that with increasing y the force required to penetrate the sand bank becomes larger.

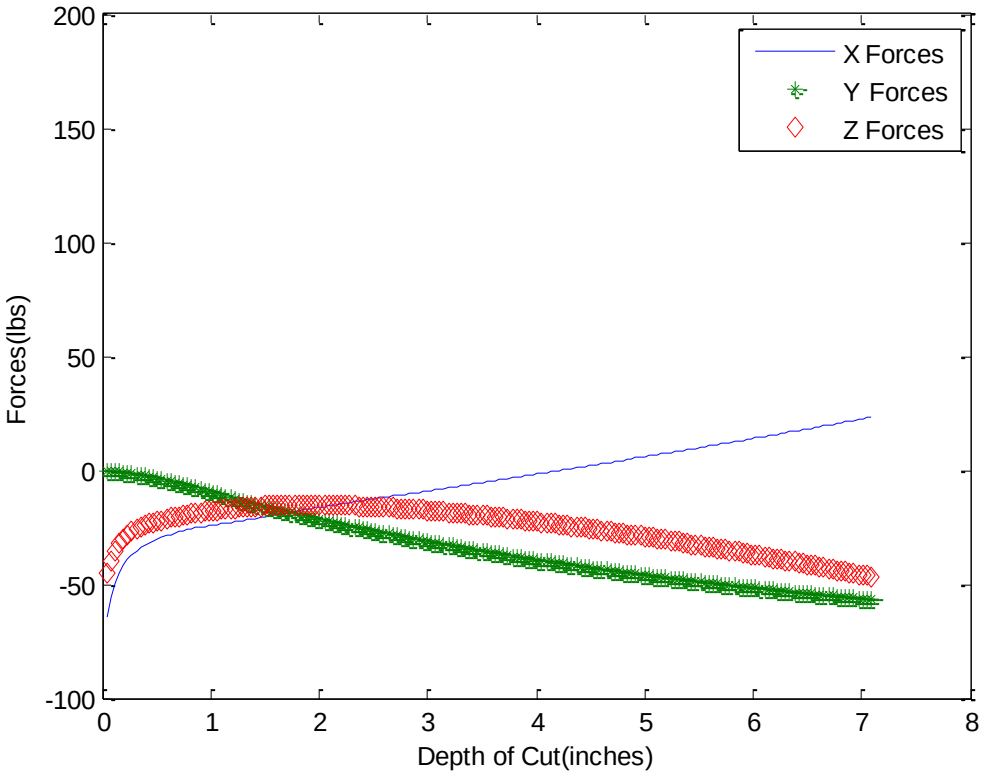

Figure 34. Effects of Cut Depth on Theoretical Forces (Undercutting)

Results Comparison

Table 4 shows the forces calculated by taking the average of overcutting/undercutting of each test on February 5. The forces for the first half of testing were overcutting and the forces on the second half of each test were undercutting. The forces determined are reasonable, but they demonstrate some variability within cases. For example, both cases 4 and 8 are theoretically equivalent, but the forces being registered are fairly different. Tests 4 and 8 were performed at 29 rpm with an 8-inch cut. Additionally, tests 1,2 and 6 should theoretically be fairly similar at 10 rpm and a 6-inch cut.

Table 4. Average Forces for Experiment (lbs)

5-Feb						
Test	X First Half	X Second	Y First	Y Second	Z First	Z Second
1	25.8	3.66	44.4	-43.1	34.8	-42.4
2	-33.2	-47.8	15.9	-12.7	17.1	-36.6
3	-30	-47	8.2	-4.06	30.6	-50.7
4	-13.9	-51.3	2.7	-8.05	70.4	-90
5	-39.6	-32.3	3.7	-9.15	-24.1	24.2
6	-19.8	-40.3	9.1	-11.4	33	-62.5
7	-37	-32	-0.57	3.97	-26.6	-6.87
8	-21.8	-39.5	5.6	-5.2	6.6	-38.4
9	-28.1	-48.9	1.9	1.3	27.3	-47.3

However, the averages of each test are quite different from each other. The range for the x forces in the first half of 1,2, and 6 range from 115 N (25.8 lbs) to 148 N (-33.2 lbs). To determine which test could possibly be an outlier the three tests were compared against each other and the testing that appeared to be the most consistent was

employed for comparison with theoretical results. These differences can be explained by the unevenness of the surface of the sand and any force due to the sliding of the dredge along the supporting rails. For cases 4 and 8 the predicted forces using theory(overcutting) were -245 N (-55.1 lbs) in the x, 66 N (14.8 lbs) in the y, and 301 N (67.7 lbs) in the z. The forces in the z for the first half of the fourth test match the theoretical predictions very closely but the other two directions are over predicted by the theoretical calculations. For the undercutting phase of test 4 and 8, the forces were 202 N (–45.4 lbs) in the x, -29.4 N (-6.62 lbs) in the y and -286 N (–64.2 lbs) in the z on average. Once again, the z seems to be the most agreeable force with the undercutting forces estimated to be -249 N (–56.0 lbs). The forces in the x direction are underestimated by 30.5 % and the forces in the y direction are overestimated by a factor of 10. However, both estimated forces fall well within the peak forces experienced during measurements. The estimated forces for 1,2, and 6 for overcutting are -192 N (-43.2 lbs) for x, 88 N (19.8 lbs) for y, and 198 N (44.4 lbs) for z. The forces using laboratory measurements on this section average about -125 N (-28.2 lbs) in the x, 103 N (23.15 lbs) for the y, and 126 N (28.4 lbs) for the z. Once again, the theory overestimated the forces measured by the force transducers in the Haynes Laboratory with only the forces in the y-direction coming close to the measured value. For the undercutting forces of 1, 2, and 6 the forces come out to be -125 N (-28.2 lbs) for x, -99.8 N (-22.4 lbs) for the y, and 209 N (-47.2 lbs) for the z with the laboratory measurements. For the theory, the forces come to -61.8 N (-13.9 lbs) for the x, -230 N (-51.6 lbs) for the y, and -164 N (-37.1 lbs) for the z. These forces turn out to be greater

than the theoretical predictions. The z force is accurate, but the x and the y to cause doubt. For cases 3 and 7 the averages for overcutting were -143 N (-33.7 lbs) for x, 16.9 N (3.81 lbs) for the y, and 9.0 N (2.0lbs) for the z and the theoretical forces were -162 N (-36.56 lbs) for the x, 29.4 N (6.62 lbs) for the y, and 177 N (39.9 lbs) for the z. The theoretical forces once again are close in two of the measurements, but the force in the z for the lab theory is much smaller than expected. This could be explained by an unintentional embedment of the cutter head at a deeper depth than intended. For the undercutting the lab forces were -176 N (-39.6 lbs) in the x, -0.22 N (-0.05 lbs) in the y , and - 128 N (-28.8 lbs) in the z. Using theory gave the results of -92.9N(-20.9 lbs) in the x, -271 N (-60.9 lbs) in the y, and -168 N (-37.7 lbs) in the z. The x and y forces are off by a wide margin, but the z shows a much closer correlation. Comparing the 5 and 9 test to theoretical values gives results of –151 N (-33.8 lbs) for the x, 12.8 N (2.9 lbs) for the y, and 6.94 N (1.56 lbs) for the z on average for the forces using the laboratory work. The theoretical forces for overcutting amounted to -206 N (-46.4 lbs) in the x, 95.6 N (21.5lbs) in the y, and 260 N (58.4 lbs) in the z. For the undercutting forces the average is -181 N (-40.6 lbs) in the x, -17.5N (-3.93 lbs) in the y, and -51.1N(-11.5 lbs) in the z. These forces correspond to the theoretical forces of -92.9 N (-20.9 lbs) in the x, -271 N (-60.9 lbs) in the y, and -168N (-37.7 lbs) in the z.

Figure 35 shows the over prediction of the forcing using the theoretical calculations. The theory consistently over predicts the average forcing but gives a good range for the peaks. The theoretical calculations overestimate the average of the experimental results by 87.8% while the undercutting is overestimated by 12.1%.

However, these forces show that the forces fall well within the peak forces seen in the measurements made at the Haynes Laboratory.

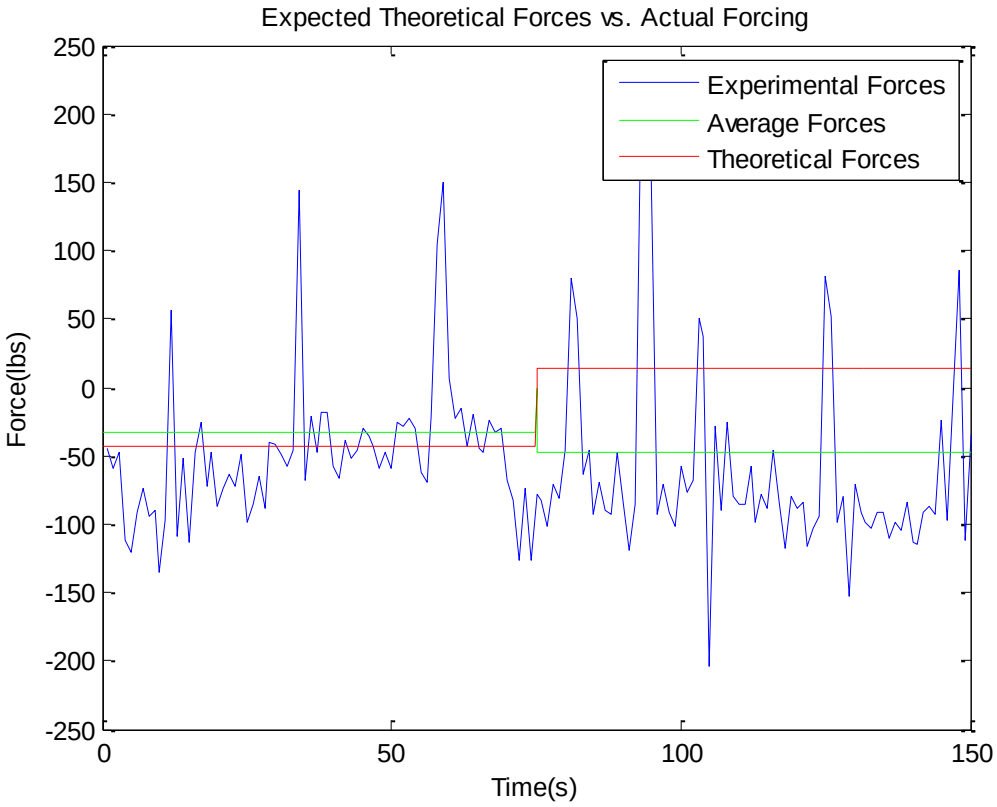

Figure 35. Comparison of Theoretical Average vs. Measured Force in the X Direction

The forces predicted by theory and the forces measured using the laboratory results are shown for the Y direction for test 1 in Figure 36. The forces for the overcutting portion are underestimated by a small margin and the theoretical forces in the undercutting portion missed the general trend shown by the experimental work. The forces estimated for each section fell within the measured forces for each case, but missed the average forces by a good

margin.

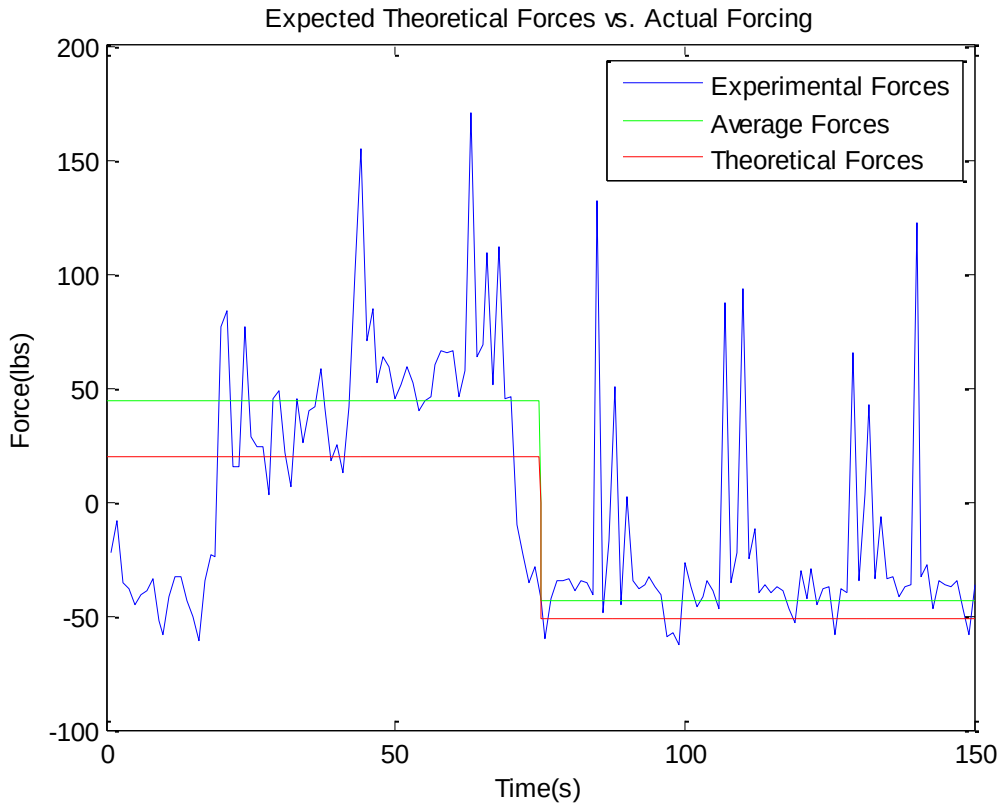

Figure 36. Comparison of Theoretical Average vs. Measured Force in the Y Direction for Test 1

The measured and theoretical forces for test 2 are contrasted in Figure 37. The forces for the whole experiment are overestimated for the average. Once again, the predicted force falls well within the range of forces measured using the experimental results..

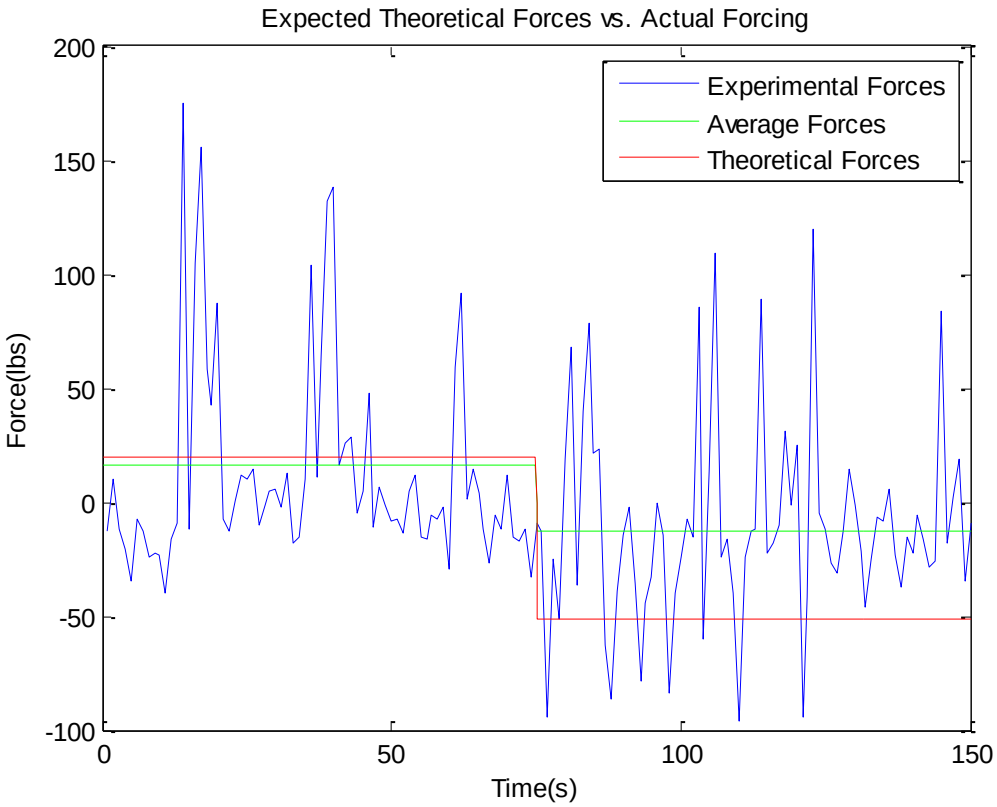

Figure 37. Comparison of Theoretical Average vs. Measured Force in the Y Direction for Test 2

The forces in the z direction for test 1 are shown in Figure 38. The average forces are close during the overcutting portion of the study and the estimated forces fall within the overall range of forcing on the plots for the undercutting portion(second half). This plot also demonstrates the wide range of values found for the forcing on the cutterhead during dredging operations.

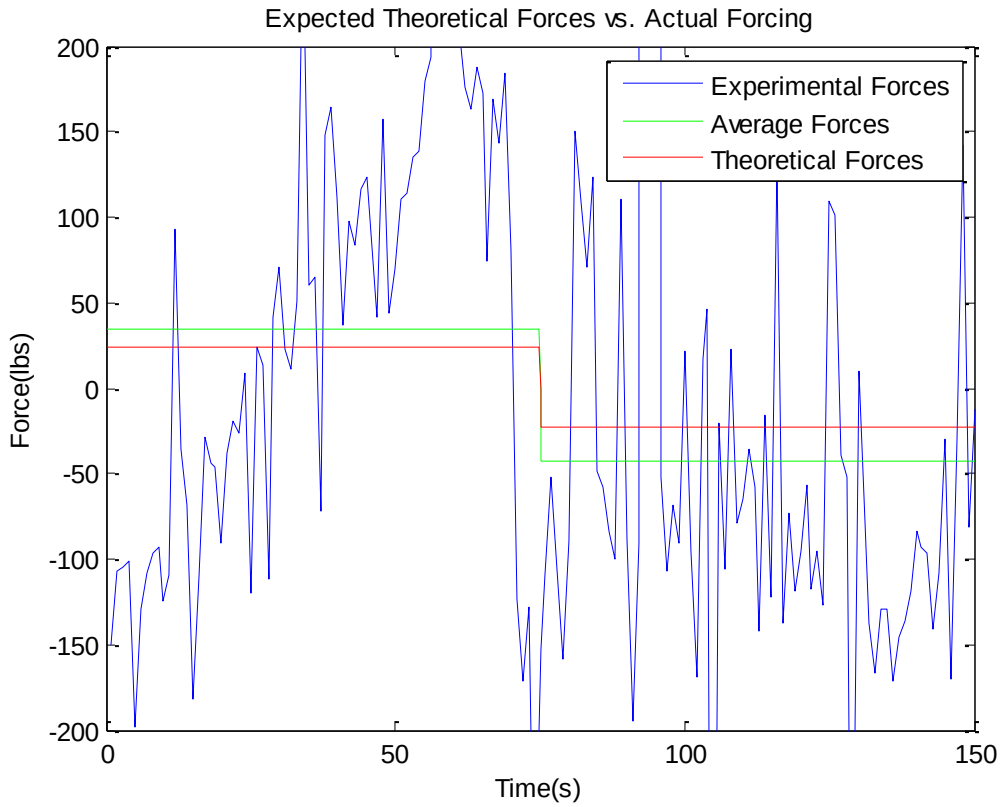

Figure 38. Comparison of Theoretical Average vs. Measured Force in the Z Direction for Test 1

Effects of RPM on Forces

The effect of the cutter rpm was much less than anticipated due to the fact that once a certain rpm is reached the forces no longer increase exponentially. The theoretical forces for varying rpm demonstrated that the difference between 29 rpm and 43.5 rpm for the given cutter model are smaller than anticipated. However, there does exist a small difference between the two cases. The results compare fairly well considering all the variables that are involved in calculating the forces on a cutter suction dredge. The

results are all within an order of magnitude of the theoretical forces, which allows for the use of either set of forces for design purposes.

CHAPTER VII

SUMMARY AND CONCLUSIONS

Summary

This thesis investigates the ability to predict the forces on a cutter head of a cutter suction dredge by theoretical calculations and compares those theoretical forces with those measured in studies previously performed. The work of Young (2009) and Glover (2002) allowed for the measurement of the forces on the dredge carriage located in the Haynes Laboratory. These studies range from simple calculations that can be made instantaneously on any operational dredge to complex calculations requiring finite element analysis.

The previous studies in this field have been fairly extensive. Although this research focuses primarily upon the efforts of Miedema (1987), the work of multiple other researchers proved valuable. The research done in the past has had quite a range of applications. The work of Van Os (1977) was crucial to the work of Miedema (1987). The previous theoretical research on the subject has often been tested with idealized cutterheads, and the use of an actual scale model cutterhead to compare to the theoretical forces supports the feasibility of these previous studies.

The new research performed in this thesis tested the Miedema (1987) theory with the forces measured by the load cells installed on the dredge carriage at the Haynes Laboratory. To determine the force on the cutter head it was assumed that the carriage was moving at constant rate across the tank. Therefore, statics can be applied to the dredge carriage as a whole, and the static equilibrium equations can be used to determine

the forcing on the load cell. These calculations were performed by Young (2009) and a slightly modified version of the program created in his research has been invaluable to the recent efforts. The theoretical forces calculated were tabulated using a MATLAB code developed to solve the theoretical equations. Several tests were used to vary the cut depth and blade rpm, and the studies were compared.

Conclusions

The verification of the measurements found on the dredge carriage model allows for further testing on the dredge carriage with different cutterheads. Additional future work could include other sediment types with varying angles of internal friction and soil/steel angles.

In the end, the forces measured by the cutterhead on the dredge carriage seem to be upheld by the theoretical results. In most cases, the forces came fairly close to that of the theory, and the discrepancies can be explained through deviation in the actual depth of the sediment as well as inconsistencies with any parameters due to the sediment. The forces estimated almost always fell within the range of forces observed through measurement but often over predicted the actual average of the force. Additionally, the forces experienced throughout the experiments demonstrated wider variation than expected. In the future, further attention to the spectral analysis can be used to determine the relative power caused by different forcing parameters on the cutter head.

The theory is also valuable in demonstrating the different phenomena occurring with increasing cut depth and angular velocity of the cutter. The results from the theory are mostly intuitive, but some of the results show phenomenon that would not be readily

apparent. The decrease in cutting force beyond certain angular velocities allowed for the determination of the prime operating speed for the particular cutter head. The smaller the forces on the cutter, the less torque the cutter drive has to provide.

Using the programs developed in the study allows for an approximation of the forces found upon an actual cutter head. The forces found using these programs can then be scaled to fit an actual cutter suction dredge and then applied to design work.

REFERENCES

Dredging Today, "DCI Cutter Suction Dredge XVIII." 2010. 14 Oct. 2010 < http://www.dredgingtoday.com>

Glover, G. J. and Randall, R.E. (2004) "*Scaling of Model Hydraulic Dredges with Application to Design of a Dredge Modeling Facility",* Journal of Dredging Engineering, Western Dredging Association (WEDA), Vol. 6, No. 2, pp 15-35.

Miedema, S.A.(1987) "The Calculation of the Cutting Forces when Cutting Water Saturated Sand, Basic Theory and Applications for 3-Dimensional Blade Movements with Periodical Varying Velocities for in Dredging Usual Excavating Elements." Ph. D Dissertation, Delft University, The Netherlands

Os, A.G. and Van Leussen, W., "Basic Research on Cutting Forces in Saturated Sand". Journal of Geotechnical Engineering, Vol. 113, No. 12, December 1987.

Turner, T. M. (1996) *Fundamentals of Hydraulic Dredging.* Second Edition. ASCE: New York.

Vlasblom, W.J. (1998) "Relation Between Cutting-, Sidewinch-, and Axial Forces for Cutter Suction Dredgers." *Proceedings of the 15th World Dredging Congress,* WODCON XV, Las Vegas, NV, pp. 275-291.

Young, D. (2009)"Forces on Laboratory Model Dredge Cutterhead." M.S. Thesis, Ocean Engineering Program, Zachry Department of Civil Engineering, Texas A&M University, College Station.

Supplementary Sources Consulted

Albar, A.(2001) "Modeling of a Bucket Wheel Dredge System for Offshore and Tin Mining." Ph. D Dissertation, Ocean Engineering Program, Zachry Department of Civil Engineering, Texas A&M University, College Station.

Randall, R.E., P. deJong, S. Sonye, N. Krippner, and J. Henriksen. "Laboratory Dredge Carriage for Modeling Dredge Operations." Ocean Engineering Program, Civil Engineering Department, Texas A&M,Proc. WODCON XVII, Orlando, Florida, USA, June 2007.

Young, D & Randall, R.(2009) "Laboratory Measurement of Forces on a Dredge Cutterhead." *Proceedings of the Western Dredging Association* , St. Louis, Missouri.

APPENDIX A

The MATLAB programs to calculate the forces from both the theory and experimental results are shown below. The first program needs only the test, run, and plotsave inputted. These variables allow the program to determine which file is wanted for the converting of the forces measured on the load cells into x, y, and z. The next programs are the theoretical force calculation programs including the programs called in the main force program.

Load Cell Conversion Program

```
%Cutting Force Calculator for six load cell configuration.
%Cutting Forces in the five load cells are
%If plotsave is 1 then the plots of Fcx Fcy and Fcz will be saved.If it is
%0 they will not.
function [avg,Fcx,Fcy,Fcz]=Conversiontoforce(test,run,plotsave)


name=[num2str(test) '_' num2str(run)]
filename=['Y:\Rusty_020510\test' name]
fid=fopen(filename);
data=fscanf(fid,'%f %f %f %f %f %f %f %f %f',[9,inf]);
%Adjust the raw data to a percentage
data=data*10;
%--------------------------------------------------------------------------
theta =30;
Waa=339.4; %Weight of Articulating arm and dredge cutterhead
%Units are in pounds
Wlad=1436; %Weight of upper and lower ladder
n=1; %n=1 for test#1 and n=16 for test #2
t=length(data)
F22=17.064;
F33=-114.29;
F44=2.153;
F55=0.729;
F66=115.01;

%Averaging the raw data
W1=mean(data(2,:));
F2=mean(data(3,:));
F3=mean(data(4,:));
F4=mean(data(5,:));
F5=mean(data(6,:));
```

```
F6=mean(data(7,:));
%Using calibrations to find actual average forces for each run
Fc1=30.2091*W1+174.9756;
F2a=30.5827*F2-82.3436;
F3a=27.9397*F3+32.4884;
F4a=28.21*F4+8.7501;
F5a=31.2517*F5-99.3691;
F6a=30*F6;
%adjusting the data
Wadj=Waa+Wlad+Fc1;
F2adj=F2a-F22;
F3adj=F3a-F33;
F4adj=F4a-F44;
F5adj=F5a-F55;
F6adj=F6a-F66;
%Separating the data out from the raw matrix
Fc1raw=data(2,:);
Fc2raw=data(3,:);
Fc3raw=data(4,:);
Fc4raw=data(5,:);
Fc5raw=data(6,:);
Fc6raw=data(7,:);
%Applying calibration data to the cells
Fc1a=30.2091*(Fc1raw)+174.9756-Wadj;
Fc2a=30.5827*Fc2raw-82.3469-F2adj;
Fc3a=27.9397*Fc3raw+32.4884-F3adj;
Fc4a=28.21*Fc4raw+8.7501-F4adj;
Fc5a=31.2517*Fc5raw-99.3691-F5adj;
Fc6a=30*Fc6raw;

%Calculation of cutting forces for each iteration
s=pi/180;
for k=1:length(Fc1a)
   Fc1=Fc1a(k);
   Fc2=Fc2a(k);
   Fc3=Fc3a(k);
   Fc4=Fc4a(k);
   Fc5=Fc5a(k);
   Fc6=Fc6a(k);
   Equmatrix=[0 0 0 -1; 0 -1 0 0; 1 0 -1 0; 0 0 -55.0212*cos(theta*s-.4556*s) 0;...
      0 0 (236.185+55.021*sin(theta*s-.4556*s)) 0; 0 -(236.185+55.021*sin...
      (theta*s-.4556*s)) 0 55.0212*cos(theta*s-.4556*s) ];
   knownforces=[-Fc1+Fc4*.00175+Fc5*.0888-Wlad-Waa; -Fc3+Fc5*.996+Fc6; -Fc2+Fc4*.9999;...
       Fc3*9.25+Fc5*9.0885-Fc6*9.125;Fc2*6.875-Fc4*61.141-Fc5*.8116;-
Fc3*6.875+Fc5*62.37669+Waa*...
       21.2992*cos(theta*s-.5237*s)-Fc6*61.675];%figure out what is here
   sol=Equmatrix\knownforces;
   Fc5x(k)=sol(1);
   Fcx(k)=sol(2);
   Fcy(k)=sol(3);
   Fcz(k)=sol(4);
end
figure(1)
```

```
fig1=plot(Fcx)
title(['X Forces ' filename])
xlabel('Time (s)');
ylabel('Force(lbs)');
figure(2)
fig2=plot(Fcy)
title(['Y Forces' filename])
xlabel('Time (s)');
ylabel('Force(lbs)');
figure(3)
plot(Fcz)
fig3=title(['Z Forces' filename] )
xlabel('Time (s)');
ylabel('Force(lbs)');
avg.xone=mean(Fcx(1:end/2));
avg.xtwo=mean(Fcx(end/2:end));
avg.yone=mean(Fcy(1:end/2));
avg.ytwo=mean(Fcy(end/2:end));
avg.zone=mean(Fcz(1:end/2));
avg.ztwo=mean(Fcz(end/2:end));
max(Fcx)
if plotsave ==1
saveas(fig1,['Y:\Rusty_020510\xforce' name],'jpg' )
saveas(fig2,['Y:\Rusty_020510\yforce' name],'jpg' )
saveas(fig3,['Y:\Rusty_020510\zforce' name],'jpg' )
end
```

Coefficient Calculation Programs

```
function [c1,c2,d1,d2]= coeff(a,b,phi,hb,hi,d,z,kmax,ki,vc,e,bpr)


[p1,p2]=porepressure(a,b,hi,z,hb,kmax,ki,vc,e,phi,d,bpr)
p3=0;
p=phi;
c1=(p1*sind(p)/sind(b)+p2*(hb/hi)*sind(a+b+p)/sind(a))*sind(a+d)/sind(a+b+d...
   +p)-p2*(hb/hi)+p3*(hb/hi);
c2=(p1*sind(p)/sind(b)+p2*(hb/hi)*sind(a+b+p)/sind(a))*cosd(a+d)/sind(a+b+d...
   +p)-p2*(hb/hi)*(cosd(a)/sind(a))+p3*(hb/hi)*cosd(a)/sind(a);
d1=(sind(p)/sind(b)+(hb/hi)*sind(a+b+p)/sind(a))*sind(a+d)/sind(a+b+d+p)-(hb/hi)...
   +p3*(hb/hi);
d2=(sind(p)/sind(b)+(hb/hi)*sind(a+b+p)/sind(a))*cosd(a+d)/sind(a+b+d+p)-(hb/hi)*cosd(a)/sind(a)...
   +p3*(hb/hi)*cosd(a)/sind(a);

function f =f(om1,om0)
om1=om1*3.14/180;
om0=om0*3.14/180;
f.one=(sin(om1)^3)/3;
f.two=(cos(om1)^3)/3-cos(om1)+2/3;
f.three=(sin(om0)^2-sin(om1)^2)*.5;
f.four=.5*(om0-om1)-(sin(2-om0)-sin(2-om1))/4;
f.five=sin(2-om1)/4;
```

```
f.six=cos(om1)-cos(om0);
```

Force Calculation Program

```
function[cnc,cca,f,g,Fst,Fvt,Fat,Mt,Fx,Fy,Fz]= forces(overunder,rpm,depthcut)
%If the cutter is overcutting two should be entered.
%If the cutter is undercutting one should be entered in overunder.
p=5;%Number of Blades on Cutter
vs=3.66/75;%haulage velocity in m/s
himax=vs*60/(rpm*p);%width of cut
iota=30;%angle of blades on cutter
z=2.5;% water depth
Bv=depthcut;%breach height
angle=35;%alpha
beta=10%30;
phi=21.65;
d=0.5*phi;
km=0.000419;%average permeability
xi=10;
e=15;%Volume strain in percent
n0=rpm;%speed of cutter in Rpm
R=.2032;%Radius of cutter in m
b=.11;%Width of Blade in m
rho=1000;%density of water
grav=9.81;%acceleration due to gravity
hb=.14913%heigth of blade in meters
vcir=2*3.14*R*n0/60;
bpr=b*cosd(iota)*cosd(xi)
vc=vcir*cosd(iota);
cnc=(p/6.28)*rho*grav*bpr*vcir*(himax^2)*e/km
cca=(p/6.28)*rho*grav*bpr*(z+10)*himax

om0=acosd(1-Bv/R);
om1=om0;
hi=himax*sind(om0)*cosd(xi);
ki=.8*km;
g=g(iota,xi,hb,hi,angle,beta,phi,d,z,km,ki,vc,e,bpr)


f=f(om1,om0)
Fst=cnc*[f.one*g.one+((-1)^overunder)*f.two*g.two]+cca*[f.three*g.three+((-
1)^overunder)*f.four*g.four];
Fvt=cnc*[-f.one*g.two+((-1)^overunder)*f.two*g.one]+cca*[-f.three*g.four+((-
1)^overunder)*f.four*g.three];
Fat=-cnc*f.five*g.five-cca*f.six*g.six;
Mt=cnc*f.five*g.one*R+cca*f.six*g.three*R;
Fx=(cosd(angle)*Fat-cosd(90-angle)*Fvt)*2.2/9.81;
Fz=(sind(angle)*Fat+sind(90-angle)*Fvt)*2.2/9.81;
Fy=((-1)^(overunder))*Fst*2.2/9.81;
```

Pore Pressure Program

```
function [p1m,p2m,fh,fv,factor]=porepressure(a,b,hi,z,hb,kmax,ki,vc,e,phi,delta,bpr)
a=deg2rad(a);
b=deg2rad(b);
phi=deg2rad(phi);
delta=deg2rad(delta);
theta1=pi/2-a-b;
theta2=a+b;
theta3=pi-b;
theta4=pi+b;
N=100;
lmax=hi/sin(b);
rhow=1;
g=9.81;
p0=0;
B=bpr;
stepl=lmax/N;
p=0;
DPMax=rhow*g*(z+10);
Flag=false;
for i=0:N
l=i*stepl+.0000000001;
s1=(lmax-l)*cos(theta1)*pi/2+(lmax-l)*sin(theta1)+hb/sin(a);
s2=l*theta2;
s3=l*theta3;
s4=(lmax-l)*theta4+0.1*hi*pi;

r1=s1/kmax;
r2=s2/kmax;
r3=s3/ki;
r4=s4/ki;
rt=1/(1/r1+1/r2+1/r3+1/r4);
dp=rhow*g*vc*e*sin(b)*rt;
  if i==N
    dp0=dp
  end
    p0=p0+dp
   if dp>DPMax
       dp=DPMax;
       Flag=true;
   end
  p=p+dp;
end



p1m=(p-dp/2)/N;
p0=(p0-dp0/2)/N;
```

```
factor=(hi/hb)^(pi/2-a*1.2)*sin(a+b)*sin(a)/sin(b)/2;
if Flag==1;
   argument=-2*factor*(p0-p1m)/p1m;
   factor=factor*exp(argument)+(1-exp(argument))
end
p2m=dp*factor

if p2m>DPMax
   p2m=DPMax;
end
   w1=p1m*hi*B/sin(b);
   w2=p2m*hb*B/sin(a);
   k2=w1*sin(phi)+sin(a+b+phi)*w2/sin(a+b+phi+delta);
   fh=k2*cos(a+delta)-w2*sin(a);
   fv=k2*cos(a+delta)-w2*cos(a);
   p1m=p1m*kmax/(rhow*g*vc*e*hi);
   p2m=p2m*kmax/(rhow*g*vc*e*hi);
   coefc=(rhow*g*(z+10))*hi*b;
   d1=fh/coefc;
   d2=fv/coefc;
   coefnc=(rhow*g*vc*e*hi^2*b)/((ki+kmax)/2);
   c1=fh/coefnc;
   c2=fv/coefnc;
```

VITA

Rusty Lee Permenter received his Bachelor of Science degree in physics and mathematics from Stephen F. Austin State University in 2008. He entered the Ocean Engineering Program at Texas A&M University in September 2008 and received his Master of Science degree in December 2010. His research interests include dredging and sediment remediation.

Mr. Permenter may be reached at the Department of Civil Engineering, c/o Dr. Robert Randall, Texas A&M University, College Station, TX 77843-3136. His email is rustylp@yahoo.com.